AD-A080 088 PRATT AND WHITNEY AIRCRAFT GROUP EAST HARTFORD CONN F/G 11/6
DEFORMATION AND FRACTURE OF ADVANCED ANISOTROPIC SUPERALLOYS.(U)
NOV 79 A F GIAMEI F44620-76-C-0028
UNCLASSIFIED PWA-FP-12637 AFOSR-TR-80-0033 NL

| OF |
AD A
080088

END
DATE FILMED
2 — 80
DDC

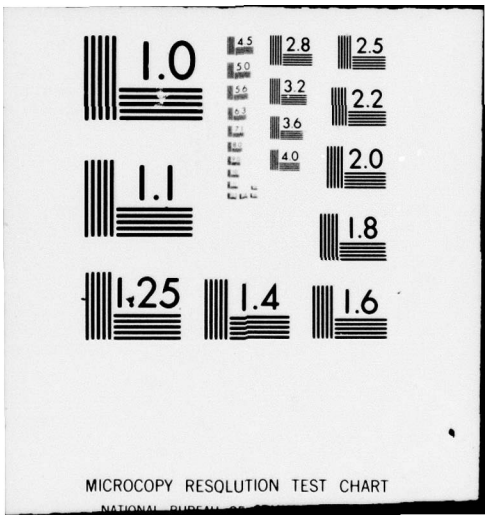
1.0
1.1
1.25
1.4
1.6
1.8
2.0
2.2
2.5
2.8
3.2
3.6
4.0
4.5
5.0
5.6
6.3
MICROCOPY RESOLUTION TEST CHART

LEVEL II

AD A080088

DDC FILE COPY

RECEIVED
JAN 31 1980
E

This document has been approved for public release and sale; its distribution is unlimited.

DEFORMATION AND FRACTURE OF ADVANCED *ANISOTROPIC SUPERALLOYS*

Approved for public release; distribution unlimited.

Final Report 10/1/78 - 9/30/79

Prepared for the
Air Force Office of Scientific Research
Building 410
Bolling Air Force Base, D.C. 20332

Prepared by: Anthony F. Giamei

Anthony F. Giamei
Principal Investigator

Approved by: R.A. Sprague

R.A. Sprague
Manager, MERL

PRATT & WHITNEY AIRCRAFT GROUP
Commercial Products Division

UNITED TECHNOLOGIES

EAST HARTFORD, CONNECTICUT

UNCLASSIFIED

SECURITY CLASSIFICATION OF THIS PAGE (When Data Entered)

19

REPORT DOCUMENTATION PAGE

READ INSTRUCTIONS BEFORE COMPLETING FORM

18 1. REPORT NUMBER: AFOSR-TR-80-0033

2. GOVT ACCESSION NO.

3. RECIPIENT'S CATALOG NUMBER

4. TITLE (and Subtitle)

6 Deformation and Fracture of Advanced Anisotropic Superalloys.

5. TYPE OF REPORT & PERIOD COVERED: Final Technical Report 1 Oct 75 - 30 Sep 79

6. PERFORMING ORG. REPORT NUMBER

7. AUTHOR(s)

10 Anthony F. Giamei

8. CONTRACT OR GRANT NUMBER(s)

15 F44620-76-C-0028

9. PERFORMING ORGANIZATION NAME AND ADDRESS

Pratt & Whitney Aircraft Group
United Technologies Corporation
East Hartford, Connecticut 06108

10. PROGRAM ELEMENT, PROJECT, TASK AREA & WORK UNIT NUMBERS

61102F
16 2306-A1
17 A1

11. CONTROLLING OFFICE NAME AND ADDRESS

Air Force Office of Scientific Research/NE
Bolling Air Force Base, D.C. 20332

12. REPORT DATE

11 November 1979

13. NUMBER OF PAGES

64

14. MONITORING AGENCY NAME & ADDRESS (if different from Controlling Office)

9 Final technical rept. 1 Oct 75 - 30 Sep 79,

15. SECURITY CLASS. (of this report)

Unclassified

15a. DECLASSIFICATION/DOWNGRADING SCHEDULE

16. DISTRIBUTION STATEMENT (of this Report)

Approved for public release - distribution unlimited

12 67

14 PWA-FP-12637

17. DISTRIBUTION STATEMENT (of the abstract entered in Block 20, if different from Report)

18. SUPPLEMENTARY NOTES

19. KEY WORDS (Continue on reverse side if necessary and identify by block number)

Single crystal superalloys, creep, deformation, Re-alloying additions, anisotropy

20. ABSTRACT (Continue on reverse side if necessary and identify by block number)

The modern single crystal superalloy baseline of Ni-5Al-2Ti-1Nb-9Cr-12W (by weight) was selected (PWA 1444). The Re/W ratio was varied from 0.0 to 1.0 as the Re + W was held constant at 12 wt %. Single crystals were grown with axial orientations of <001>, <110>, and <111> from four different alloys and were fully heat treated (gamma prime solution + age). An additional alloy was made at 4Ta/4W/4Re in the three high symmetry orientations. Test specimens of the compressive and tensile creep/rupture design were obtained by sectioning or electrochemical machining. Creep data were obtained in

DD FORM 1 JAN 73 1473 EDITION OF 1 NOV 65 IS OBSOLETE

UNCLASSIFIED

SECURITY CLASSIFICATION OF THIS PAGE (When Data Entered)

287 500

JOB

tension and compression with temperature/stress combinations of 816°C/650 Mpa, 899°C/380 MPa, 982°C/220 MPa and 1066°C/138 MPa (1500°F/94 ksi, 1650°F/55 ksi, 1800°F/32 ksi and 1950°F/20 ksi).

Crystals were characterized by chemical analysis, optical metallography and crystallographic orientation determination by the Laue method. Aging studies were carried out at 816°C (1500°F), 899°C (1650°F), 982°C (1800°F) and 1066°C (1950°F). The Re content was found to systematically and substantially refine the gamma prime particle size. Transmission electron microscopy was carried out after 0.20% creep strain at 899°C (1650°F). The primary slip system was consistently (111) <110> for <001> and <110> oriented specimens but (100) <110> slip was found for the <111> oriented tensile and compressive samples at 0% Re. Higher Re levels showed a lesser tendency for cube slip.

The Re addition substantially strengthens all three orientations tested, particularly <111>. The gamma prime particle size refinement increases the potency of the Re solid solution strengthening effect. Fine gamma prime particle sizes may be less favorable to cube cross slip, a fundamental characteristic of gamma prime. Low stacking fault energy in the matrix at high rhenium content appears to make dislocation constriction difficult, as well as climb or cross-slip. Stress coarsening of gamma prime occurs in <100> and <110> oriented creep specimens, but at a rate which decreases with Re content.

TABLE OF CONTENTS

1.0 ABSTRACT

Under the first year effort in this program, the anisotropy of tensile and compressive properties was studied for $\gamma / \gamma' + \delta$, a directionally-solidified eutectic alloy under evaluation for turbine blade application in advanced gas turbine engines. The dependence of the δ twinning behavior on the direction of loading was identified as a key reason for the anisotropy in properties and relatively low transverse tensile ductility for this alloy system. As far as is currently known, this was the first study that demonstrated the role of anisotropy in the plastic properties of the reinforcing phase on the mechanical properties of the directionally-solidified eutectic in which it resides.

For the second year of this program, the anisotropy in creep-rupture behavior was studied for single crystal nickel-base superalloys. Single crystal superalloys are currently being intensively evaluated at P&WA for application as turbine blades in advanced military engines and, because of the similarity in processing methods to those for directionally-solidified (columnar-grained) superalloys, are expected to see service in the 1980's well in advance of the potential introduction of air-cooled DS eutectic components. To date, single crystals have demonstrated a 27°C (50°F) temperature advantage over columnar-grained superalloys and have the potential for a 55°C (100°F) advantage.

For the third year of this program the mechanisms of Re strengthening in single crystal γ / γ' alloys was studied. Earlier experiments indicated significant γ' particle size refinement and high temperature strengthening in model superalloys. In the work reported for the past twelve months, rhenium has been added to a high strength single crystal version of MAR-M200. Samples of wide ranging orientation have been tested under creep conditions in the 871-982°C (1600-1800°F) temperature range. Metallography, replication, TEM and microprobe analysis have been used to determine the strengthening mechanism. The γ' particle size and interparticle spacing were measured as they may relate to various strengthening theories.

A fourth year of effort has been completed which was a logical extension of the Re modified single crystal work. Modified MAR-M200 with 0-6 wt % Re was tested in tensile and compressive creep in $<001>$, $<110>$ and $<111>$ orientation. Crystals were grown with various W/Ta ratios and examined by electron channeling Laue back reflection and omega scanning diffractometry to characterize crystal perfection. Further microstructural characterization was carried out by TEM and replication before and after deformation. The temperature range of testing was extended downward to 816°C (1500°F) and upward to 1066°C (1950°F).

2.0 INTRODUCTION

The trend in the development of creep-resistant wrought and cast alloys for gas turbine applications has been and continues to be in the direction of aligned microstructures. Oxide-dispersion strengthened alloys, directionally-solidified superalloys, and directionally-solidified eutectics all have microstructures which are aligned to provide maximum creep properties in the direction of principal component loading. The mechanical properties of these materials in directions not parallel to the aligned microstructure, however, are generally lower. That is, the properties are anisotropic.

As part of the first year effort in this program, under Air Force Contract F44620-76-C-0028, the anisotropy of tensile and compressive properties was studied for γ / γ' + δ, a directionally-solidified eutectic alloy under evaluation for turbine blade application in advanced gas turbine engines. Results to date have clearly demonstrated the strong orientation dependence of the twinning behavior of the reinforcing δ (Ni_3Cb) phase. The ability of the δ phase to plastically deform by twinning has been shown to depend on the sign of the applied stress as well as the angle between the loading axis and the eutectic freezing direction. These results can account in large part for the marked orientation dependence of ductility for this directionally solidified eutectic alloy.

Other advanced, anisotropic materials currently under intensive development at Pratt & Whitney Aircraft include γ' Ni3 (Al, Ti) precipitation-hardened nickel-base superalloy single crystals. Single crystal superalloy turbine blades offer a significant temperature advantage over the best current alloys and are expected to see service in advanced military engines in the 1980s. The crystal anisotropy can be utilized in terms of matching the orientation (elastic modulus) to the application in order to minimize vibration.

For the second year of this program, therefore, the anisotropy in creep-rupture behavior was studied for superalloy single crystals. Previous work on this subject (References 1 through 3, Section 5.0) has shown that the creep rates and rupture lives at relatively low temperatures are a strong function of the angle between the loading axis and the crystallographic axes of the alloy. In addition, it was demonstrated that the anistropy in creep properties depends strongly on temperature, with the orientation dependence being considerably different at 857°C (1575°F) compared to 760°C (1400°F).

The second year was designed to establish the anisotropy in creep behavior of single crystals of an advanced nickel-base superalloy at the higher temperatures likely to be encountered in advanced military applications. Creep-rupture tests were performed on superalloy specimens where the angle between the loading axis and the crystallographic axes was systematically varied. Differences in creep rate and rupture life for all crystal orientations were correlated with the operative slip systems as well as other important microstructural factors. The results can be compared with the earlier data generated at lower temperatures in order to highlight the mechanisms responsible for the temperature dependence of the anisotropy.

To summarize the observations on the orientation dependence of MAR-M200 single crystal creep at 760°C (1400°F), it was found that shear of the γ / γ' structure occurs by the glide of loosely coupled intrinsic/extrinsic fault pairs with a net Burgers vector of a $\langle 112 \rangle$. The orientation dependence of both the rate and extent of primary creep correlates with the Schmid factors and multiplicity of slip for $\{111\}\langle 112 \rangle$ systems. It has also been shown that strain hardening due to intersecting slip is necessary to obtain the transition from primary to steady-state creep.

As mentioned previously, the orientation dependence of MAR-M200 single crystal creep behavior is dependent on temperature. At 857°C (1575°F) it was found that shear of the gamma prime precipitate by pairs of (a/2) $\langle 110 \rangle$ dislocations controlled deformation in both primary and steady-state creep. In contrast to the 760°C (1400°F) primary creep behavior, where the highest primary creep rates and primary creep strains were measured along the [001] - [111] line, the highest steady-state creep rates at 857°C (1575°F) are measured along the line between [001] and [011]. Differences in the amount of creep among these specimens were minimal when compared to the large orientation dependence of primary creep found at 760°C (1400°F).

The difference of primary and steady-state creep behavior between 760 and 857°C (1400 and 1575°F) was attributed to the change in deformation mechanisms at the two temperatures. At 760°C (1400°F), where primary creep occurs by (a/2) $\langle 112 \rangle$ slip, a short incubation period, required to generate the operative (a/2) $\langle 112 \rangle$ dislocations by limited (a/2) $\langle 110 \rangle$ dislocation interactions, is followed by a rapid, almost primary creep rate which is dependent on crystal orientation. At 857°C (1575°F), where both primary and steady-state creep occur by (a/2) $\langle 110 \rangle$ slip, no incubation period is present, and the primary creep rate decreases continuously with time, with the amount of primary creep being relatively independent of orientation.

Single crystal Ni-base superalloys are undergoing extensive development for use in advanced gas turbine engines. This significant step allows the turbine blade designer an unusual degree of flexibility in materials properties. Recent advances in single crystal alloys provide higher melting temperatures, improved oxidation/corrosion resistance, better coatability, more efficient heat treatment, improved castability and greater stress or temperature capability. This combined with significant improvements in single crystal solidification processing offers the opportunity for improved performance at lower costs.

One of the most interesting aspects of single crystals is their versatility. Pure metal or solid solution alloy crystals are very soft with extensive easy glide and must be handled with great care to prevent recrystallization. On the other hand, the cast Ni-base superalloy crystals with their closely spaced array of coherent (and high volume fraction) γ' precipitate particles exhibit high yield strengths of ~900 MPa (130 ksi) at room temperature and are resistant to recrystallization. Unlike most materials furthermore, the superalloy crystal flow stress does not decay rapidly with temperature; often these crystals are actually stronger at 800°C (1472°F) than at room temperature.

One of the most striking examples of the versatility of single crystals in gas turbine design is the crystal anisotropy. The high multiplicity of octahedral slip and the absence of cube slip for the [001] tensile direction make this orientation ideal for creep limited applications at the high end of the intermediate temperature range. The low elastic modulus along [001] makes this an excellent choice if high thermal fatigue or low cycle fatigue (strain controlled) lives are desirable. The low octahedral Schmid factor along [111] makes this the most creep resistant orientation in most superalloys at the low end of the intermediate temperature range (where cube slip is not a factor). The very high [111] elastic modulus makes this an excellent choice for vibration or high cycle fatigue (stress controlled) limited applications.

The element rhenium has recently been shown to be a potent strengthener of nickel-base superalloys. This alloying addition combined with single crystal technology offers significant promise for advanced turbine airfoil materials. Yet little is known about the strengthening mechanism of rhenium in nickel-base superalloys. The objective of the third year program was to elucidate the basic Re strengthening effect.

It appears that most of the Re resides in the γ matrix of Ni-base superalloys. Re is a large heavy atom which could be a potent solid γ solution strengthener. Re is partioned away from γ' during precipitate particle growth. The slow apparent diffusion characteristics of the Re necessitate a finer than normal γ' particle size which seems to be more resistant to coarsening.

The primary objective of the third year of effort was to gather microstructural and behavioral information which would lead to the determination of the rhenium strengthening mechanism for a modern single crystal superalloy base such as Ni/5Al/2Ti/1Nb/9Cr/12W. This alloy will be designated 1444. Solidification processing state-of-the-art has advanced to the point where such alloys can be grown with high single crystal quality and dendritic structures which are fine enough that chemical homogeneity can be achieved by solution heat treatment within a few hours. Recent evidence suggests this can contribute significantly to high temperature strength and creep resistance in that all the γ' is utilized on a fine scale leading to a higher effective volume fraction of strengthening phase.

Previous work indicates that the anisotropy of single crystal creep behavior is significantly different at the three temperatures of 760, 857 and 982°C (1400, 1575 and 1800°F). The properties of superalloys change markedly with temperature in this temperature range and data on creep has been sorely lacking, particularly for off - [100] orientations. Recent advances in solidification processing make it easier to obtain such orientations and this technology could be utilized in the follow-on to the current program. Some microstructural work was done near 900°C (1650°F) to establish the relative importance of {111} <110>, {111} <112>, {001} <110>, {001} <100> and even {110} <110> or possibly {112} <110> in Re bearing crystals.

Clearly, the Re effect cannot be optimized or utilized until the source of strengthening is understood in some detail. Initial seeding experiments for obtaining the precise <110> and <111> growth axes in bars were highly successful. Samples were machined for creep testing in both compression and tension. Initial computer monitored compressive creep results proved to be highly reproducible. Thin foil techniques were established for alloy 1444 + Re. Subsequent TEM work and replica work lead to an improved understanding of the Re strengthening mechanism.

The objective of the fourth (and final) year of effort was to elucidate the rhenium strengthening mechanism(s) by extending the temperature range of testing downwards to 816°C (1500°F) and upwards to 1066°C (1950°F). This temperature range corresponds fully with that of interest for a turbine blade application. Also, more compressive creep data was to be generated to compare to tension. This work was concentrated at 899°C (1650°F). The high symmetry <100>, <110> and <111> crystals were grown, solution heat treated, coating simulation heat treated, precipitation aged, machined and mechanically tested.

Additional crystal characterization work was completed. Extensive gamma prime solution heat treated and aged specimens were analyzed by electron metallography for coarsening kinetics at four temperatures and four rhenium levels. $\theta/2\theta$ and ω/χ x-ray diffraction scans were done to reveal more information about crystal perfection. Along these lines, an additional composition of 4Ta/4W/4Re was grown in the three corners of the stereographic triangle to see if the presence of Ta substantially affected the mechanical properties or crystal perfection of alloys such as 1444. Ta was selected because it generally improves the oxidation resistance, leads to higher intermediate temperature strength and has a distribution coefficient during solidification which is < 1, vs. > 1 for both W and Re.

Additional clarification was sought on alloy stability at 6 wt % Re and on the influence of Re on stress coarsening. Transmission electron microscopy work was done to look carefully at the γ / γ' interface for evidence of fine, third phase precipitates or dislocation networks in the fully heat treated microstructure.

Yield strength data was collected in compression from room temperature to 982°C (1800°F) for several combinations of rhenium level and crystal orientation. The extensive creep data of the past two years was organized into tables showing creep ductility in all orientations tested and into the Larson-Miller framework (4).

The single crystals were to be grown by previously established techniques (5-6). The gamma prime particle size data can be compared to coarsening theory (7). These results will allow a valid comparison to be made with other strengthening theories based on particle cutting (8, 9) or dislocation anisotropy (10) or other ordered compounds (11) or the full gamut of superalloy strengthening mechanisms (12-21).

3.0 Status

3.1 Mechanical Properties

3.1.1 Creep Curves

Under the current effort, the primary objective was to fill in the test matrix including composition, orientation and temperature wherever possible. We have concentrated on expanding the data base at 899°C (1650°F) in tension and compression. We have also expanded the test temperature range down to 816°C (1500°F) and up to 1066°C (1950°F). No testing was done this year at 982°C (1800°F) since this was adequately covered in 1977 and 1978. The complete test matrix for 1977-1979 is presented in Table I. It will be noted that a new alloy has been added with 4Ta/4W/4Re by weight. The total % refractory metal addition is still the constant 12%, as before.

The specimen preparation and test methods have been previously described. The tensile creep data are presented in Figures 3-1 through 3-7 and Table II. Most of the tensile creep specimens were duplicate tests with little scatter, although some testing was done singly and some in triplicate. In general, the results on 0 and 6% Re at 816°C (1500°F)/650 MPa (94 ksi) and those with the 4/4/4 alloy at 899°C (1650°F)/380 MPa (55 ksi) are similar to previously presented test results for 0, 2, 4 and 6% Re at 899°C (1650°F) and 982°C (1800°F)/220 MPa (32 ksi) in that rhenium monotonically decreases the creep rate as it is added, particularly in the case of <111> oriented specimens. Also, the <001> is generally the strongest, and <111> the weakest. The 4/4/4 specimens generally fall between the 2% Re and 4% Re added to PWA 1444 (at the expense of W). Typical scatter is shown in Figure 3-3. Creep ductility is given in Table III.

The results at 1066°C (1950°F)/138 MPa (20 ksi) are obviously different from those obtained at lower temperature. First, there is considerably more scatter in the data, and secondly, the Re effect is reversed in that (above 2%) higher Re levels lead to shorter lives in <100>, <110> and <111>. The reason for this effect is that the microstructure is unstable, as we shall see.

Compressive creep curves are shown in Figures 3-8 through 3-12. The stress levels were the same as those used in the tensile creep tests, but the minimum creep rate (MCR) is generally smaller and the time to a given strain longer for compression, see Table III. The reproducibility in MCR in compressive creep is excellent, as shown in Table IV.

The extreme long times anticipated to 2% strain at the temperature selected for most compressive data (899°C or 1650°F) for the <110> orientation led us to carry out the <110> compressive creep testing at a lower temperature, higher stress condition for the 4 Re levels, see Figure 3-8. Again, the Re effect is monotonic and the lives are extensive in compression. Figures 3-9 through 3-11 are given for the study temperature of 899°C (1650°F). The Re strengthening effect is seen to be monotonic for <001>, <110> and <111>. The <110> and <111> Re strengthening effects are quite pronounced compared to <001>. The <110> orientation is particularly strong in com-

pression. The final Figure in this sequence is 3-12 which shows that at 1066°C (1950°F)/138 MPa (20 ksi) the primary creep strain and a value for MCR can be obtained even from the strain history typical of specimens obtained for thin foil analysis in some cases.

3.1.2 Larson-Miller Curves

The most effective way to present the data generated from 1977-1979 is by means of Larson-Miller plots where the stress for rupture (or 1% creep) is plotted against the Larson-Miller parameter, which combines the effects of temperature and time. These plots are presented in Figures 3-13 through 3-21. In these plots, the average of multiple tests has been used wherever possible. Figure 3-13 shows the effect of orientation on tensile creep rupture behavior in the base alloy. Note that < 001 > is always the strongest orientation. Figures 3-14 and 3-15 show multiple strain contours for < 001 > at 0 and 6% Re in the case of tensile creep. Note that C=20 leads to straight lines on this logarithmic plot primarily for the case of rupture, with curvature predominant at the lower strains. A careful comparison of these diagrams shows that the largest Re effect is at low to intermediate strain values at intermediate temperatures.

Figure 3-16 is comparable to 3-13 except that the time to 1% is used rather than the time to rupture. A similar plot is shown in Figure 3-17 for the base PWA 1444 alloy with all three major orientations, but in compression. A comparison of Figure 3-16 with 3-17 reveals that the previously reported lower creep rate in compression by 1X-2X is true generally for < 100 > and < 111 > , but the < 110 > orientation is in the range 4X-6X more creep resistant in compression.

Figures 3-18 through 3-20 show the chemical effects at 2, 4 and 6% Re. All of these plots are for time to rupture. Comparison with Figure 3-13 shows the monotonic improvement in creep behavior with Re additions at all but the highest test temperatures. Insufficient data were collected to allow this type of plot for the 4/4/4 alloy, as several temperatures and stresses are required.

Figure 3-21 shows a plot derived from Larson-Miller data in slightly more useful engineering form. This plot of stress required to bring about 1% creep in 100 hr. versus temperature for the baseline 1444 alloy and the 6% Re addition. Here the high temperature phase instability can be seen to cause a cross-over in the curves. In order for such alloys to be useful over the full temperature range, the phase instability must be identified, and then eliminated, e.g., by an Nv approach (22), or possibly by homogenization during high temperature heat treatment.

3.1.3 Compressive Yield Strength

In superalloys, with more conventional grain structures there is rarely any asymmetry in yield behavior in tension versus compression. It was considered important to the potential use of materials similar to those under study, to investigate the yielding behavior as a function of orientation and Re level. It was convenient to prepare small squared compression specimens with aspect ratios in the range 3:1 to 4:1 at the

three corners of the stereographic triangle and to subject these to repeated yielding to a plastic strain of 0.2% at a strain rate of 5% per min. The results are shown in Tables V - VII and Figures 3-22 to 3-24. The five temperatures selected were from room temperature to 982°C (1800°F). The room temperature test was repeated at the end to indicate the extent of any work hardening. This varies from about 21 MPa (3 ksi) for 100 to 35 MPa (5 ksi) in 111 for each test. The results are shown for 0, 2, 4 and 6% Re as well as the 4/4/4 alloy.

There are three very interesting effects which should be pointed out in these yielding data. First, the 0% Re is unusually strong at 816°C (1500°F). Secondly, the Re generally effects the higher temperature properties. Finally, the <111> orientation is strengthened significantly by Re over the entire temperature range. This is a key observation with respect to the strengthening mechanism.

3.2 Microstructure

3.2.1 Gamma Prime Coarsening

Previous reports in this series have shown that γ' stress coarsens in the 1444 alloy base. A series of aging treatments were given to the alloy 1444 and Re modified 1444 after solution heat treatment. Single crystals were used and the (001) face was subsequently examined by surface replication using the electron microscope. The isothermal aging plan is shown in Table VIII. Some replications are shown in Figures 3-25 through 3-28 for 1950°F/2hr and 1500°F/296hr. Note that the γ' particles are much more regular at the higher aging temperature and at higher Re levels. The newest data are for 2 and 4 Re at all temperatures as well as 0 and 6 Re at 1500°F and 1950°F. Some previous conditions were reprinted at a higher magnification for a more accurate analysis of particle size.

The overall kinetic results have been depicted graphically in Figure 3-29 through 3-32. It can be seen that the γ' coarsening rate decreases with decreasing temperature, both in intercept (at time = 1 hr) and slope. The higher temperature coarsening rates vary as $t^{1/3}$, indicating diffusion control, while at lower temperature the slopes clearly decrease to about $t^{1/4}$, indicating interface control (7). It is particularly significant that these observations hold true for 0, 2, 4 and 6 wt % Re.

Two techniques were used to measure the particle sizes. One was to measure the area fraction γ', A_A, (by a systematic grid point counting method), count the particle density, N_A, and knowing the particle shape as cuboidal, relate these as follows:

$$A_A = N_A A_P \tag{3-1}$$

and the area per particle is given as:

$$A_P = \overline{D^2} \tag{3-2}$$

Thus, we have:

$$D = \sqrt{A_A/N_A} \tag{3-3}$$

These measurements were quite tedious when carried out manually. Attempts were made to carry out quantative metallography on prints from replicas using an automated computerized system. However, reference to Figure 3-25 through 3-28 indicates a lack of sufficient discrimination between the γ matrix and the γ' particles. Most of the contrast is at the γ / γ' interface. An alternate method was to use a line intercept technique. Since the specimens were (001) oriented, square arrays of square particles were generally observed. If a line is laid parallel to either edge of such an array and the number of particles, Np, as well as the cumulative line length in each particle, Lp, is recorded, the particle diameter is given by:

$$D = \frac{Lp}{Np} \sqrt[3]{V_V} = \frac{Lp}{Np} \sqrt[3]{\bullet A_A} \simeq 0.86 \frac{Lp}{Np} \qquad (3\text{-}4)$$

To enhance the accuracy, measurements were taken along two mutually perpendicular cube directions, and 10-20 particles were included in the intercept length in each of these directions. Higher magnifications were made of some previously reported conditions and improved measurements were taken.

The probable change in mechanism mentioned during low vs. high temperature γ' coarsening may be responsible for a lack of a straight line relationship in the thermal activation analysis given in Figure 3-33. In this case the 6 Re seems to behave differently than 0-4. It can at least be seen that the time to reach a given particle size can vary from 3X to 1000X, depending on temperature and Re level. Additional analysis has been carried out in Figure 3-34, where the particle sizes at constant aging time are plotted vs. Re level. This isochromal plot also shows complexities typical of multiple mechanisms, but at least it can be seen that the presence of Re leads to a 2X to 3X reduction in particle size for a given exposure time.

3.2.2 Gamma Prime Layering

There is some tendency for a small number of gamma prime particles to locally link up during isothermal aging to form rectangular platelets, but this effect is greatly exaggerated by stress. We have previously reported results for 1800°F (982°C) testing near $<001>$. The current work investigated this phenomenon with Re added and for the high modulus orientations. These results are reported in Table IX and Figures 3-35 through 3-37. Layering, or stress coarsening, was observed at high temperature in the $<001>$ and $<110>$ orientation, but not for $<111>$. This is consistent with general superalloy behavior. The Re effect on stress coarsening is evident in Figure 3-36, with finer layers at 6 Re than at zero. The γ' layering which was observed was always perpendicular to the tensile axis.

3.2.3 Sigma Phase Formation

Some of the high exposure temperature (1950°F) creep rupture specimens exhibited sigma phase formation. This can be detected as thin platelets on octahedral planes by optical metallography as in Figure

3-38. This phase was observed for long exposure times with the 4 and 6% Re alloys. The specimens were taken from the shoulder region of creep rupture samples. Note that the phase is located in the cores of dendrites.

The sigma phase was also detected by TEM at the threaded end of the following creep-rupture specimens: <111> 1444 + 4 Re, 1950°F/20 ksi/ 242 hr and <001> 1444 + 6 Re, 1950°F/20 ksi/86 hr. The occurrence of this phase is not critically dependent on stress, but rather temperature and residual microsegregation. TEM analysis indicated the formation of a regular Widmanstatten pattern.

The <111> specimen mentioned above was also submitted for STEM analysis to verify the sigma identification and determine the composition. The area investigated and the spectral analysis are shown in Figure 3.39 and the chemical analysis results are shown in Table X. The σ is surrounded by γ' which was also analyzed. The matrix and some γ' particles were also checked. A spatial resolution of 0.2 μm (2000 A) was achieved in the above work. The γ is essentially (Ni, Cr, W, Re), the γ' is basically $(Ni, Cr)_3$ (Al, Ti, W) and the σ can be regarded as $(Ni, W)_3$ (Cr, Re). Without the σ present, the Re level in γ would be much higher (~ 12%). Note the complete lack of Re in γ' even in this complex alloy.

3.2.4 Crystal Quality

In the current year of this deformation study program, particular attention was paid to crystal quality. The purpose was to try to establish methods to quantify crystal imperfections and then to correlate overall quality with alloy chemistry and finally creep or yield behavior. The simplest method was the x-ray back reflection Laue spot quality. With a 0.030 inch (0.076 cm) diameter collimator, and the standard 3 cm sample to film distance, spots were normally obtained which were extremely sharp when the bottom end of a bar was carefully cut and electropolished. The top end typically exhibited asterism to the extent of 1-2°. A traverse across a 0.6 inch (1.52 cm) diameter bar led to long range orientation differences of 0-2° at the bottom and 1-3° at the top end.

A more quantitative technique was developed for superalloy crystal assessment, namely ω - X scanning or a "rocking curve" analysis where an oriented crystal is rocked through the Bragg angle while the detector sits stationary in a decoupled single crystal diffractometer. Using a carefully aligned goniometer, a crystal face is placed near the Bragg condition and the Fe filtered Co radiation is received through medium slits (so as not to exclude any diffraction from entering the detector). The crystal must be carefully prepared so as to avoid any serious extinction effects. The diffracted beam is received into a scintillation counter and the output is transmitted through a pulse height analyzer into a rate meter, digitized scalar or intensity vs. angle plotter. The crystal is manually moved through θ (ω) and X and the detector is manually moved through 2θ in alternation until an absolute maximum in intensity is achieved. The crystals were of such high quality that even at the lowest power settings (20 Kv, 6 ma) the intensity received at the detector was so high that 50% or 90% filters were used

for Co K α in the diffracted beam. The crystals are generally "ideally imperfect" in that they rarely exhibit extinction to any serious extent, but do diffract very strongly. From this optimal alignment position, a $\theta/2\theta$ scan or an ω scan can be made with ease. The shapes of both of these curves give us the required detailed information about crystal quality. The χ variable can be changed (prior to several ω scans) to make a $\chi - \omega$ map. However this was found to provide little additional information. The system had much more vertical (2-4°) than horizontal (0.5-1°) divergence, so χ was not a variable of great sensitivity.

The lower end of all bars was generally of very high quality. The top ends were studied as a function of chemistry, orientation and heat treatment. Alloy chemistry was not found to be an important variable, as Re additions seemed to have little effect and the 4Re, 4Ta, 4W alloy was comparable to the 1444 base in ω scan breadth. The $\theta/2\theta$ peaks were generally sharp and will be presented in the next section. They were always recorded to check the crystal surface preparation. Heat treatment showed little noticeable effect on the ω breadth. The controlling variable was clearly crystal orientation. The ω breadths were 0.5-1° for (200) or (220), but 0.2-0.3° for the (111) reflections. (All references here are to planes cut perpendicular to the growth axis). These results are presented in Figure 3-40. The <100> crystal quality was deteriorated by the presence of thermal or mechanical convection during solidification. There may be substructure growing from the melt and there may be polygonization during the directional cooling, but heat treatment does not lead to any more or less substructure.

The final tool used to localize the 0.5-1° substructure was the use of an electron channeling method. An attachment to an electron microprobe allows the precise determination of relative orientation to within 0.1-0.2°. Figure 3-41 shows the (001) transverse dendritic structure in the backscatter mode. In the secondary electron image, definite contrast is seen as associated with small groups (1-5) of dendrites. This suggests some type of solidification substructure is being generated during crystal growth. The channeling patterns are taken before and after a 200 μm translation (about 1 dendrite) and a significant misorientation, typically a fraction of a degree, is detected.

3.2.5 γ / γ' Misfit

We have previously pointed out δ fringes in the TEM work on alloys containing Re. In the current x-ray diffraction work, it was noted that the (002) reflection was severely asymmetric in alloys containing Re, particularly after full heat treatment, see Figure 3-42. The (001) and (003) γ' superlattice reflections were always narrow Gaussian shaped curves with no tails to the low angle side. The γ' (001) and (003) allowed for a lattice parameter determination which matched the sharp intense components of the (002) peak. Thus, the γ phase has a larger lattice parameter and we have a case of negative misfit as follows:

$$\delta = \frac{a_{\gamma'} - a_{\gamma}}{a_{\gamma}} < 0 \qquad (3.5)$$

This is consistent with higher Re solubility in γ than γ' and the presumption that Re expands the γ phase. Note that the γ(002) peak is smeared so that α_1 and α_2 are not resolved. This is probably due to misfit strains or Re gradients (or both). Using Co Kα and an approximate 2θ position for the γ phase, we calculate a misfit of approximately -0.3%. This is larger than most superalloys and in the opposite sense.

The baseline 1444 alloy also showed some low angle (200) tail, but not quite so pronounced in $\Delta 2\theta$ or in amplitude. No long low angle tails were seen in the as cast condition in any alloy. There were two cases of full resolution of the $\gamma K\alpha_1$ peak (with $\gamma K\alpha_2$ under $\gamma' K\alpha_1$). These were the (222) reflection at 120^o 2θ in the 1444 + 6 Re (fully heat treated) and (002) reflection in the 4Re/4Ta/4W alloy after full HT. In both cases the intensity of the $\gamma K\alpha_1$ peak was about 40% of the $\gamma' K\alpha_1$, consistent with a γ' volume fraction of 60-70%, assuming comparable average atomic scattering factors due to the heavy substitution. The misfit was more clearly -.3% (since there was a clear separation of 0.2^o 2θ and very little broadening) as given by:

$$\lambda = 2d\sin\theta \tag{3.6}$$

$$0 = 2d\cos\theta\Delta\theta + 2\Delta d\sin\theta \tag{3.7}$$

$$\frac{\Delta d}{d} = \frac{\Delta a}{a} = -\tan\theta\Delta\theta = \frac{1.73 \times 0.1}{(180/\pi)} \tag{3.8}$$

In percent:

$$\frac{\Delta a}{a} = \frac{-1.73 \times 100}{57} \cong -0.3\% \tag{3.9}$$

Two attempts were made to further characterize the γ / γ' interface by TEM. We had previously examined thin foils of fully heat treated undeformed 1444 with (001) sections, and found these to be practically dislocation free. In an attempt to see misfit dislocations at the γ / γ' interface, a foil was prepared of (001) oriented fully HT 1444 + 6 Re. The result, somewhat surprisingly was again a clean foil with very few dislocations.

The same material was examined in a (111) foil to determine the nature of the previously reported fringes near the γ / γ' interfaces. The fringe contrast increased with Re level. It was positively concluded that the contrast around the particles was due to a small misfit and was exhibited in the form of δ fringes since:

1. The contrast was absent when the operating diffraction vector was contained in the interface.

2. The optimum fringe contrast was obtained when the deviation parameter, s was slightly negative.

3. When S >> 0, only the extreme fringes were visible.

4. The fringe spacing was dependent upon the extinction distance in a rather complex fashion.

3.2.6 Slip Structure

We have previously tested TEM data indicating the active slip system to be $\{111\}$ $< 110 >$ at 1800°F/32 ksi in tension, at least in the base alloy without rhenium additions. The deformation was homogeneous at that temperature, since there was very little rotation in the $< 001 >$ crystal axes. We then showed that as Re was increased from 0 to 6% at 1650°F/55 ksi, the γ' particles were finer and fringes were much more pronounced at the higher Re levels. Foil sections on the most probable $\{111\}$ slip plane from these $<001>$ oriented specimens taken to 0.2% strain were analyzed assuming octahedral slip.

Table XI indicates the new data for $< 110 >$ and $< 111 >$ axial deformation at 1650°F/55 ksi in tension and compression for 0-6% Re. Dodecahedral plane sections were added for the $<110>$ specimens for convenience of analysis, and cube plane sections were added for the $<111>$ specimens since there was some suspicion of cube slip, namely $\{001\}$ $< 110 >$. Complete analyses are presented for 0 and 6 Re in tension in Figure 3-43 and 3-44, while the general appearance is shown for 2 and 4 Re in compression in Figure 3-45. Standard analysis techniques identified the dislocation tangent vectors (solving the relplane two dimensional diffraction pattern) and the dislocation slip vectors (disappearing contrast at $g \cdot b = 0$, where g is the operating diffraction vector in a two beam condition such as that shown in Figure 3-45). Note that dotted vectors are out of plane and b_m = b mixed. When b and g are labelled simultaneously, b is still parallel to g , which is labelled specifically. Three to eight vectors were analyzed for each condition. There can be no doubt that $< 110 >$ is the operational slip vector (although a few stacking faults were seen at 1650°F, indicating at least some $< 112 >$ shear). The long dislocation lengths of edge character in $<111>$ TA at 0 Re for (001) foils verify cube slip. These are seen to decrease with increasing Re. Most dislocations were actually of the mixed type and very few screws were observed. The dislocations were generally in the γ phase or at the γ / γ' interfaces. The observed dislocation density at 0.2% strain was ideal for analysis, although normally this was a condition prior to the formation of extensive networks, presumably still in primary rather than steady state creep.

TABLE I - CREEP TEST MATRIX

Orientation	% Re	1500°F/ 94 ksi	1650°F/ 55 ksi	1800°F/ 32 ksi	1950°F/ 20 ksi
< 001 >	0	2T	4T, 4C	29T, 2C	2T, 1C
	2	-	3T, 1C	3T	2T
	4	-	2T, 1C	2T	2T
	6	2T	2T, 1C	2T	2T
	4/4/4	-	2T	-	-
<110>	0	2T, 1C	2T, 1C	-	2T
	2	1C	2T, 1C	-	2T
	4	1C	2T	-	2T
	6	2T, 1C	2T	-	2T
	4/4/4	-	2T, 1C	-	-
<111>	0	2T	3T, 1C	-	2T
	2	-	2T, 1C	-	2T
	4	-	2T, 1C	-	2T
	6	2T	2T, 1C	-	2T
	4/4/4	-	2T	-	-

NOTE: T = Tensile Creep
C = Compressive creep
3T = Three tensile creep tests
4/4/4 = 4Ta + 4Re + 4W

TABLE II - TENSILE CREEP DUCTILITY

Average results given as (prior creep, measured strain to failure, RA) in %.

Orientation	% Re	1500°F 94 ksi	1650°F 55 ksi	1800°F 32 ksi	1950°F 20 ksi
<001>	0	12.6,14.7,22.6	16.9,21.5,34.8	N.A.,17,N.A.	5.8,17.5,50.0
	2	-	15.1,18.9,21.0	N.A.,30,N.A.	6.9,13.8,40.0
	4	-	12.3,16.4,19.9	N.A.,31,N.A.	5.3,13.5,30.5
	6	13.3,17.0,17.7	13.7,17.2,17.4	N.A.,22,N.A.	7.5,15.5,31.7
	4/4/4	-	9.0,19.5,27.4	-	-
<110>	0	7.5,35.9,49.5*	5.0,20.4,30.3	-	2.1,7.5,7.5
	2	-	7.1,15.4,28.7	-	2.8,11.1,18.5
	4	-	8.6,27.7,36.3	-	2.7,11.0,30.9
	6	8.9,33.6,62.2	3.1,14.1,31.8	-	4.6,6.6,32.1
	4/4/4	-	4.2,7.5,6.9	-	-
<111>	0	12.8,26.7,28.5	20.0,22.7,27.0*	-	8.2,11.6,12.8
	2	-	17.8,21.1,22.9	-	7.9,13.7,15.0
	4	-	10.4,10.6,9.6	-	6.6,12.1,14.8
	6	14.9,18.4,20.7	13.5,15.6,16.7*	-	11.5,17.8,17.2
	4/4/4	-	21.2,25.2,24.8	-	-

* One or more specimens failed on loading or outside the guage region and have not been included in the averages.

N.A. = Not available; data from 1977 work; very ductile in 28/28 specimens for 0 Re and 7/7 specimens with Re added.

TABLE III - MINIMUM CREEP RATES

Results quoted in compression/tension/ratio in $\left[10^{-4}\ \text{in/in/hr}\right]$

Orientation	% Re	1500°F 94 ksi	1650°F 55 ksi	1800°F 32 ksi	1950°F 20 ksi
<001>	0	-/2.75/-	1.26/1.25/1.01	0.70/1.70/0.41	-/0.71/-
	2	2.84/-/-	0.54/1.06/0.51	-/0.62/-	-/0.72/-
	4	0.70/-/-	0.27/0.86/0.31	-/0.88/-	-/0.56/-
	6	-/2.25/-	0.24/0.61/0.39	-/0.47/-	-/2.29/-
<110>	0	10/62/0.16	0.56/3.04/0.18	-	-/0.80/-
	2	-	0.25/0.53/0.47	-	-/0.53/-
	4	-	-/0.51/-	-	-/3.03/-
	6	0.53/2.67/0.20	-/0.24/-	-	-/2.70/-
<111>	0	-/412/-	50/25/2.0	-	-/1.70/-
	2	-	7.9/5.2/1.52	-	-/0.97/-
	4	-	1.59/1.76/0.90	-	-/0/-
	6	-/13.0/-	0.70/1.0/0.70	-	-/1.28/-

TABLE IV - MINIMUM CREEP RATE REPRODUCIBILITY

Results quoted as average $\pm$ 1/2 (range) for compression/tension

Orientation	% Re	1650°F/ 55 ksi	1800°F/ 32 ksi
<001>	0	1.26 $\pm$ .03/1.25 $\pm$ .14	0.70 $\pm$ .15/1.70 $\pm$ .95
	2	0.54/1.06 $\pm$ .01	-/0.62 $\pm$ .12
	4	0.27/0.86 $\pm$ .01	-/0.88 $\pm$ .02
	6	0.24/0.61 $\pm$ .08	-/0.47 $\pm$ .09
	4/4/4	-/1.36 $\pm$ .24	-
<110>	0	0.56/3.04 $\pm$ .01	-
	2	0.25/0.53 $\pm$ .14	-
	4	-/0.51 $\pm$ .01	-
	6	-/0.24 $\pm$ .12	-
	4/4/4	-/1.55 $\pm$ .35	-
<111>	0	50/25 $\pm$ 6	-
	2	7.9/5.2 $\pm$ .2	-
	4	1.59/1.76	-
	6	0.70/1.0 $\pm$ .1	-
	4/4/4	-/4.9 $\pm$ .7	-

TABLE V

PWA 1444 COMPRESSIVE YIELD STRENGTH PROPERTIES (KSI)

Strain	Orientation	Re Level	Test Temperature °F 70	800	1500	1650	1800	70
P.L.	[001](010)	0	141.0	135.3	96.1	76.9	42.5	146.5
0.02			144.1	137.3	111.8	83.3	58.3	151.4
0.20			145.3	139.4	160.2	128.1	87.7	157.1
P.L.	[001](010)	2	145.3	142.0	122.5	77.5	57.9	159.5
0.02			148.6	144.4	132.5	90.8	66.8	164.5
0.20			151.6	144.8	161.2	133.9	92.1	165.9
P.L.	[001](010)	4	139.3	140.7	106.7	92.3	54.6	157.9
0.02			144.6	141.7	128.8	104.4	68.1	162.6
0.20			150.2	143.2	163.0	133.5	94.6	166.6
P.L.	[001](010)	6	132.5	131.4	97.1	75.0	67.9	153.4
0.02			136.4	134.4	116.2	89.2	72.1	158.4
0.20			145.3	136.0	153.8	129.9	95.9	160.6
P.L.	[001](010)	4/4/4	135.2	136.5	101.9	73.9	33.1	150.5
0.02			141.1	137.2	112.7	85.3	51.5	155.2
0.20			142.9	138.8	155.6	122.7	86.3	155.6

NOTE:

1) 4/4/4 = PWA 1444 + 4 Re + 4 Ta + 4 W

2) Strain Rate = 5%/min

3) Material H.T. 2350 F/4 hr/AC + 1975 F/4 hr/AC + 1600 F/32 hr/AC

4) P.L. = Proportionality Limit

TABLE VI

PWA 1444 COMPRESSIVE YIELD STRENGTH PROPERTIES (KSI)

Strain	Orientation	Re Level	Test Temperature °F 70	800	1500	1650	1800	70
P.L.	[011](011)	0	152.5	145.8	141.7	84.0	67.2	155.4
0.02			159.4	146.7	147.1	97.7	71.7	159.0
0.20			163.2	144.7	166.9	120.6	86.6	161.8
P.L.	[011](011)	2	144.6	147.6	140.3	88.3	67.3	166.3
0.02			152.5	148.0	142.0	100.5	75.2	168.8
0.20			160.6	149.6	146.8	123.8	89.3	172.8
P.L.	[011](011)	4	151.2	149.2	148.1	81.2	69.1	174.0
0.02			156.5	157.0	152.1	91.7	80.3	177.5
0.20			168.9	158.5	158.0	132.3	95.9	180.3
P.L.	[011](011)	6	128.4	132.4	124.1	96.6	71.5	150.7
0.02			138.2	133.6	126.7	104.0	79.0	153.4
0.20			145.1	134.0	127.9	124.1	92.9	155.8
P.L.	[011](011)	6	152.3	143.4	135.0	84.1	80.8	161.9
0.02			156.3	144.5	136.0	108.8	86.8	163.9
0.20			157.6	144.8	142.2	138.0	103.9	166.0
P.L.	[011](011)	4/4/4	156.1	153.2	122.3	79.5	66.4	163.9
0.02			161.7	153.4	138.9	96.3	77.6	166.3
0.20			169.2	154.3	167.8	134.6	97.8	167.5

NOTE:

1) 4/4/4 = PWA 1444 + 4 Re + 4 Ta + 4 W

2) Strain Rate = 5%/min

3) Material H.T. 2350 F/4 hr/AC + 1975 F/4 hr/AC + 1600 F/32 hr/AC

4) P.L. = Proportionality Limit

TABLE VII

PWA 1444 COMPRESSIVE YIELD STRENGTH PROPERTIES (KSI)

Strain	Orientation	Re Level	Test Temperature °F 70	800	1500	1650	1800	70
P.L.	[111](011)	0	130.5	112.4	89.4	68.6	47.5	164.7
0.02			140.3	112.4	110.3	76.3	55.5	175.9
0.20			151.6	113.3	114.3	87.1	60.4	180.2
P.L.	[111](011)	2	141.2	119.7	116.6	76.3	54.4	169.5
0.02			150.6	120.6	120.3	84.9	61.5	180.0
0.20			161.7	121.1	124.3	95.1	66.0	183.1
P.L.	[111](011)	4	156.0	127.8	120.8	83.8	62.2	179.5
0.02			160.4	127.8	125.9	94.3	69.0	188.2
0.20			164.5	129.1	131.3	102.1	72.4	187.8
P.L.	[111](011)	6	162.2	133.2	126.1	91.6	71.8	183.1
0.02			165.6	134.5	129.2	100.0	78.3	186.3
0.20			167.0	134.9	139.4	110.5	82.0	185.7
P.L.	[111](011)	4/4/4	158.2	129.8	103.2	84.0	63.6	182.2
0.02			161.1	128.8	125.6	91.8	69.4	183.6
0.20			163.7	129.5	125.4	106.5	79.6	183.4

NOTE:

1) 4/4/4 = PWA 1444 + 4 Re + 4 Ta + 4 W

2) Strain Rate = 5%/min

3) Material H.T. 2350 F/4 hr/AC + 1975 F/4 hr/AC + 1600 F/32 hr/AC

4) P.L. = Proportionality Limit

TABLE VIII - ISOTHERMAL AGING PLAN

Time (hr):	0.5	2.0	8.0	16	32	148	296
Temperature (°F)							
1950	X	X	X	X			
1800	X	X	X		X		
1650		X	X		X	X	
1500			X		X	X	X

Procedure: (001) Specimens oriented, cut, solution heat treated (2350°F/4 hr/FC) + 2350°F/0.5 hr/WQ + age/WQ for 0, 2, 4 and 6% Re. Replicas were made and photographed from 10Kx to 25 Kx. Specimens were also documented in the solution heat treated condition (with water quench) for all Re levels studied.

Note: *The two step solution heat treatment* is referred to as 2350°F/4.5 hr/WQ in Figure 3.29-3.32.

TABLE IX - STRESS COARSENING

Orientation	Wt % Re	Temp./Stress/Life (°F/ksi/hr)	γ' Morphology
[001]	6	1500/94/211	Cuboidal
[001]	6	1650/55/316	Cuboidal
[001]	6	1800/32/322	Elongated
[001]	6	1950/20/98	Elongated
[001]	0	1950/20/156	Coarse Elongated
[110]	6	1950/20/49	Elongated
[111]	6	1950/20/126	Irregular

NOTE: Replicas taken on longitudinal sections (containing tensile axis) in shoulder region of creep-rupture specimens after failure.

TABLE X - PHASE COMPOSITION BY STEM FOR 1444 + 4 Re CREEP EXPOSED AT 1950°F

Phase	Location	Elements (wt %) Al	Ti	Cr	Ni	W	Re	Total
γ matrix	1	0.5	0.7	14.0	61.7	17.8	5.3	100.0
particle	23	4.4	2.1	4.6	68.4	20.5	-	100.0
Agglomerated γ'	2	4.8	2.5	3.2	80.0	9.5	-	100.0
σ platelet	3	1.9	0.5	3.7	24.6	36.7	32.6	100.0

TABLE XI - THIN FOIL MATRIX

Orientation	% Re	Foil Sections	1650°F/ 55 ksi	1800°F/ 32 ksi	Other
<001>	0	K, φ	1T,1F	4T,2C,4F	As cast;fully heat treated
	2	φ	1T,1F	-	-
	4	φ	1T,1F	-	-
	6	φ	1T,1F	-	Fully heat treated
<110>	0	D, φ	1T,2F	-	-
	2	D, φ	1C,2F	-	-
	4	D, φ	1C	-	-
	6	D, φ	1T,2F	-	-
<111>	0	K, φ	1T,3F	-	-
	2	K, φ	1C,1F	-	-
	4	K, φ	1C	-	1950°F/20 ksi - shoulder
	6	K, φ	1T,2F	-	-

Notes:

K = Cube, φ = Octahedral, D = Dodecahedral

T = Tension, C = Compression, F = Good Foils

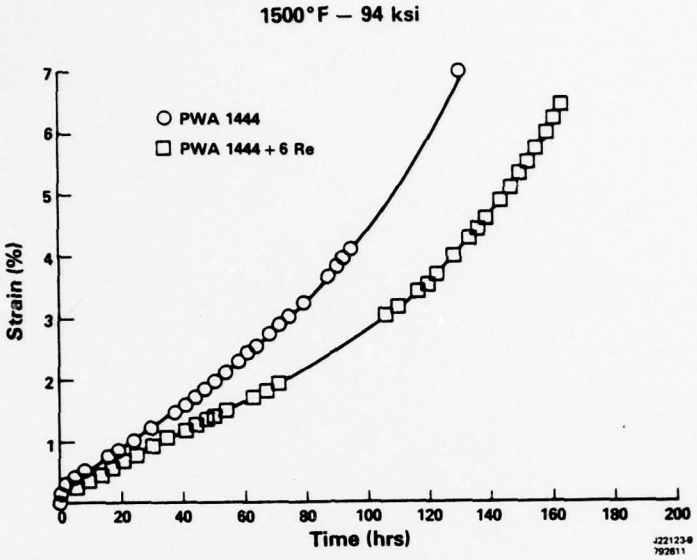

Figure 3-1 [001] Tensile Creep Curves for Alloy 1444 and 1444 + 6 Re at 1500°F/94 Ksi

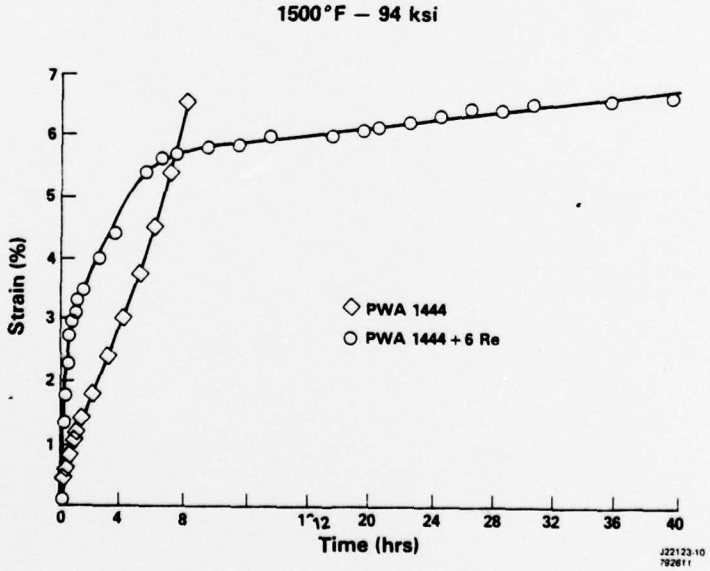

Figure 3-2 [110] Tensile Creep Curves for Alloiy 1444 and 1444 + 6 Re at 1500°F/94 Ksi

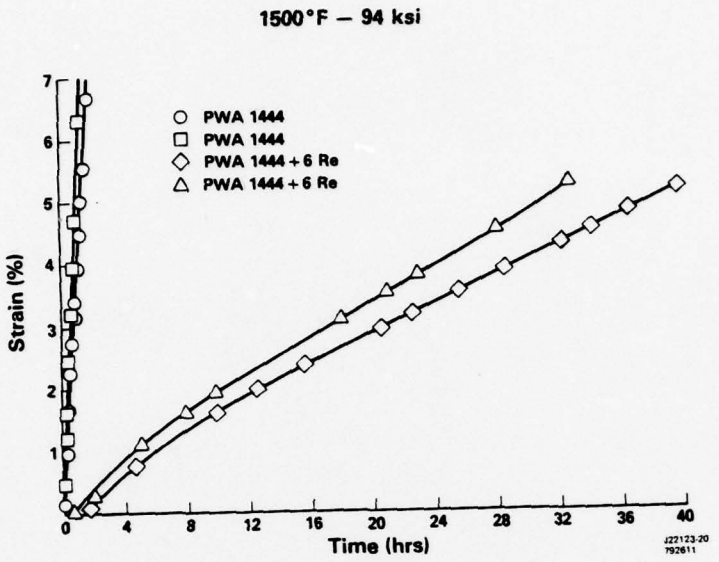

Figure 3-3 [111] Tensile Creep Curves Showing Reproducibility in Alloy 1444 and 1444 + 6 Re at 1500°F/94 Ksi

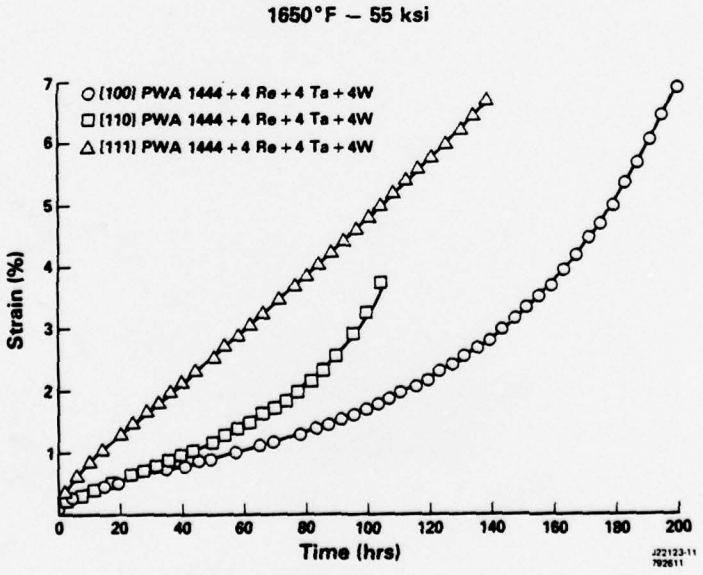

Figure 3-4 4 Ta/4 W/4 Re Modification to 1444 Shows Typical Tensile Creep Anisotropy at 1650°F/55 Ksi

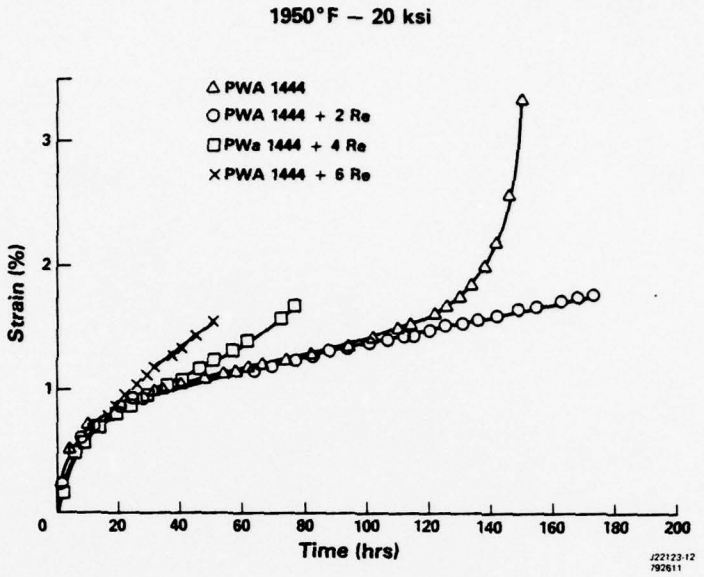

Figure 3-5 [001] Tensile Creep Curves at 1950°F/20 Ksi for All Re Levels Investigated

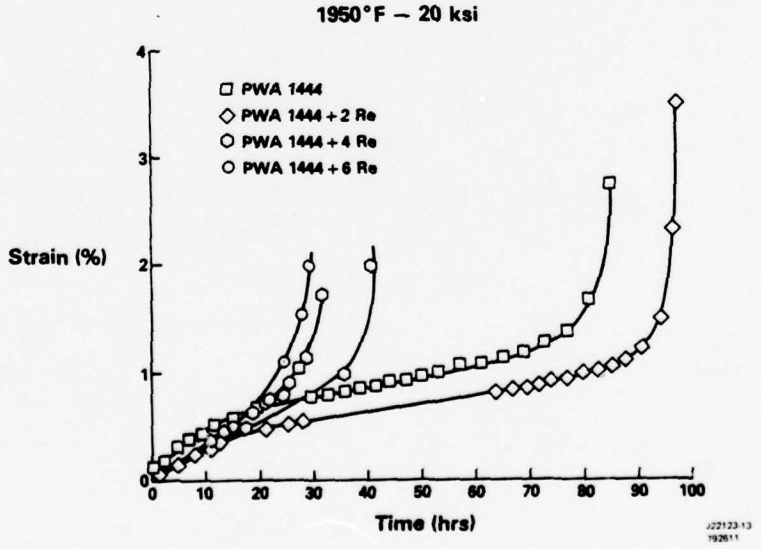

Figure 3-6 [110] Tensile Creep Curves at 1950°F/20 Ksi for All Re Levels Investigated

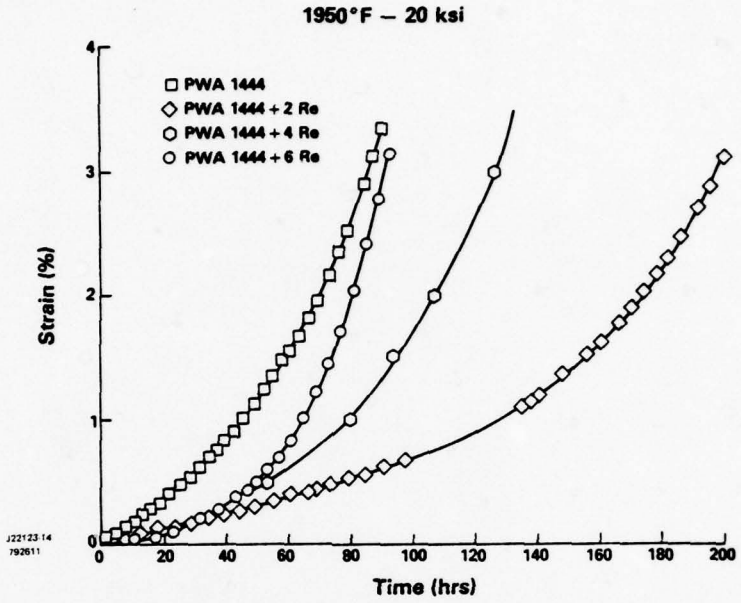

Figure 3-7 [111] Tensile Creep Curves at 1950°F/20 Ksi for All Re Levels Investigated

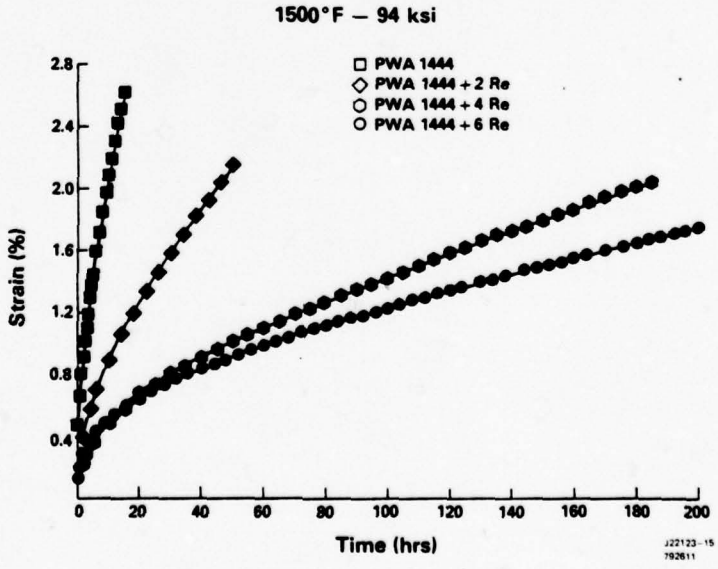

Figure 3-8 [110] Compressive Creep Curves at 1500°F/94 Ksi for All Re Levels Investigated

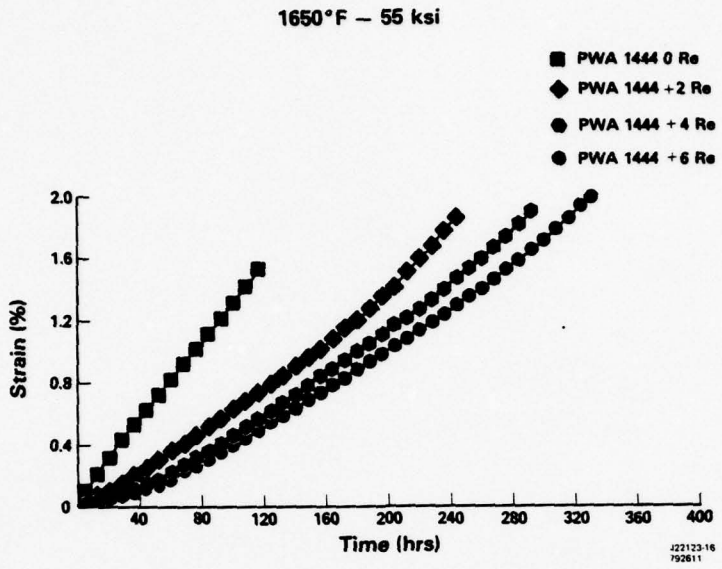

Figure 3-9 [001] Compressive Creep Curves at 1650°F/55 Ksi for All Re Levels Investigated

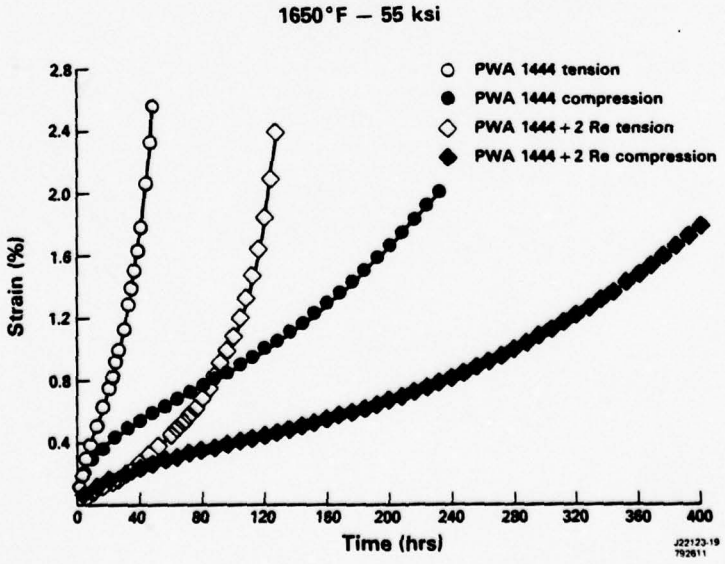

Figure 3-10 [110] Compressive Creep Curves at 1650°F/55 Ksi for All Re Levels Investigated

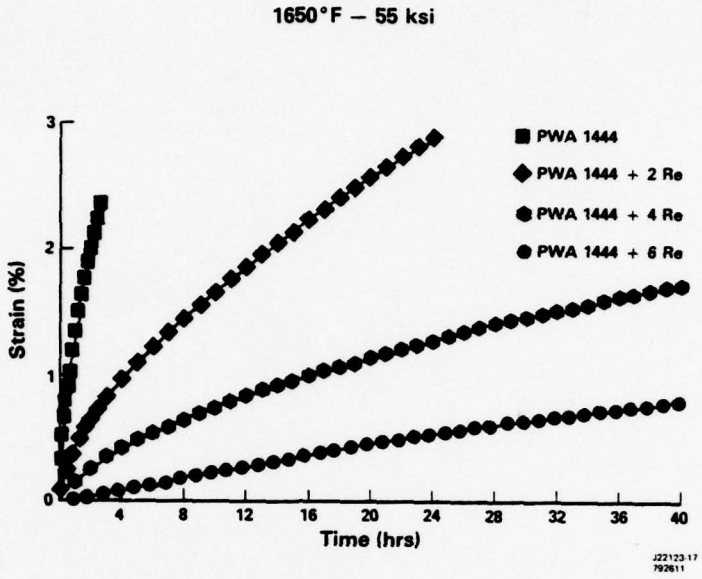

Figure 3-11 [111] Compressive Creep Curves at 1650°F/55 Ksi for All Re Levels Investigated

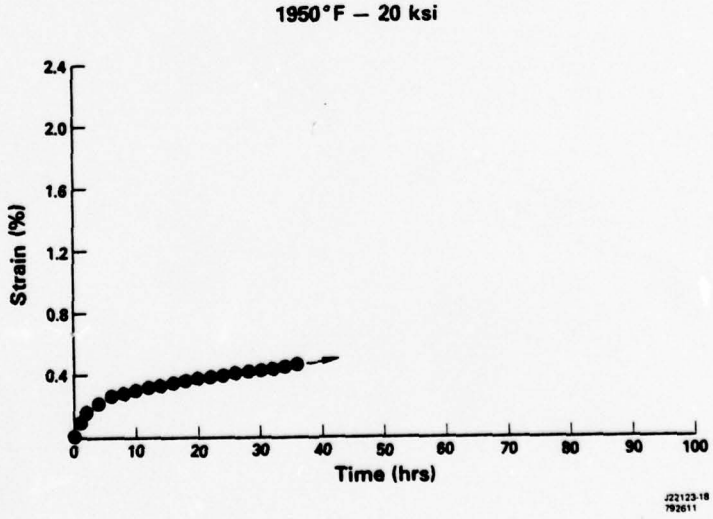

Figure 3-12 Initial Compressive Creep Data for [001] Alloy 1444 at 1950/20 Ksi. Note small magnitude of primary creep strain.

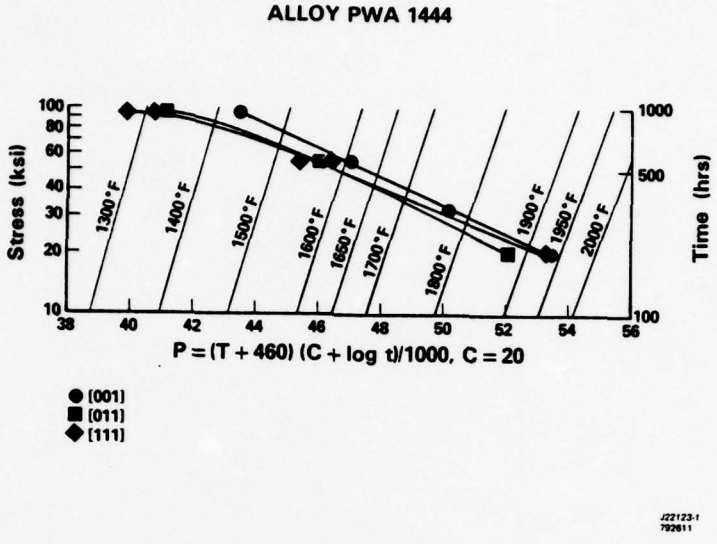

Figure 3-13 Larson-Miller Plots of High Symmetry Orientations of Alloy 1444 for Failure Condition.

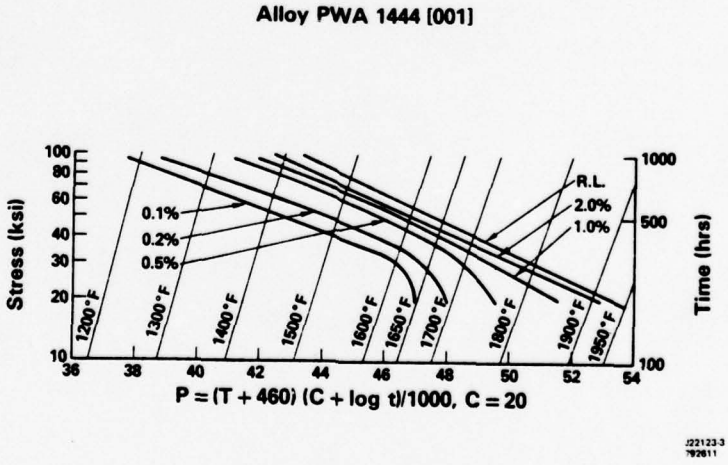

Figure 3-14 Larson-Miller Multiple Strain Contours for [001] Alloy 1444 in Tensile Creep-Rupture

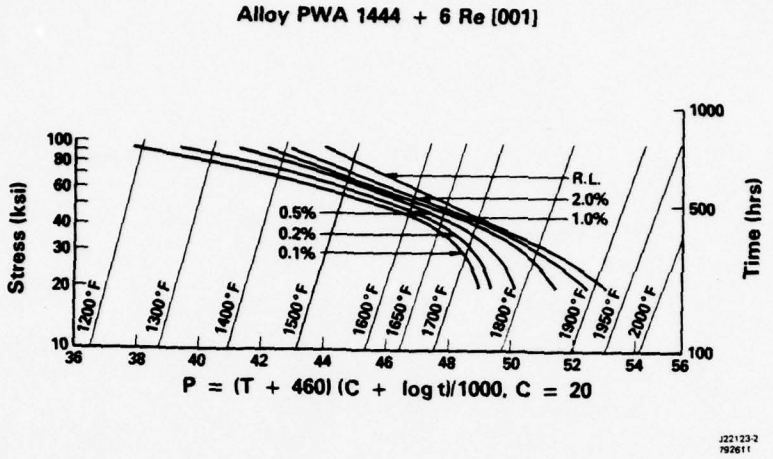

Figure 3-15 Larson-Miller Multiple Strain Contours for [001] Alloy 1444 + 6 Re in Tensile Creep-Rupture

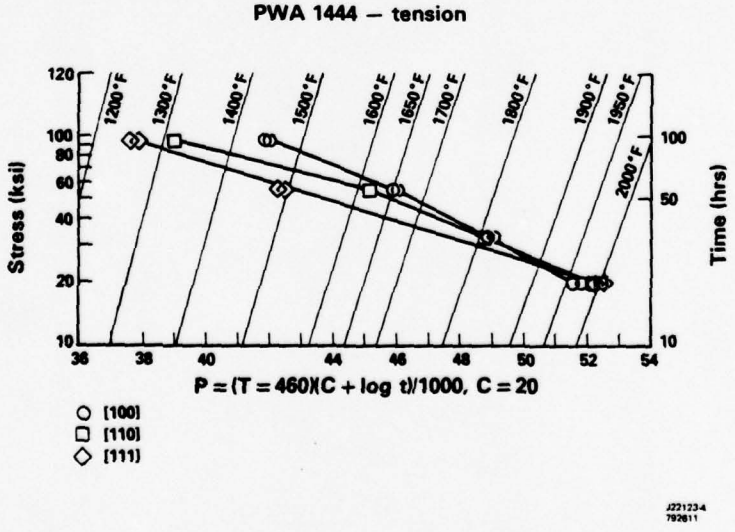

Figure 3-16 Larson-Miller Plots of High Symmetry Orientations of Alloy 1444 for Time to 1% Tensile Creep

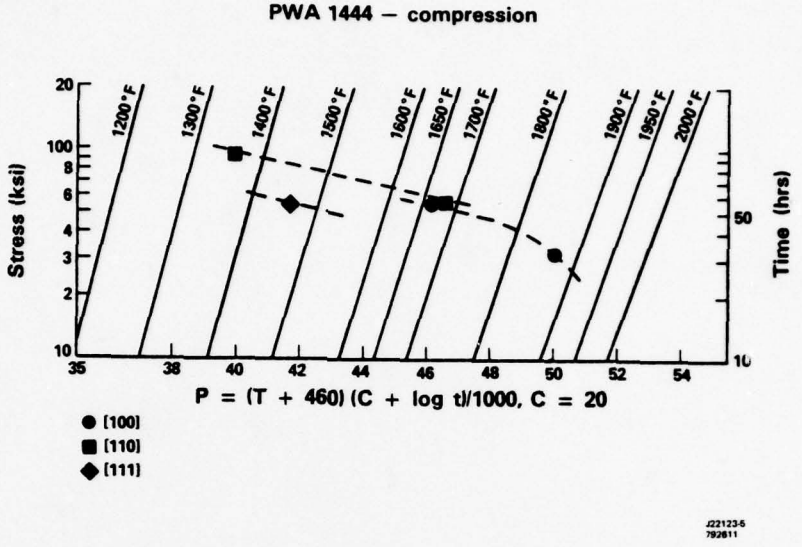

Figure 3-17 Larson-Miller Plots of High Symmetry Orientations of Alloy 1444 for Time to 1% Compressive Creep

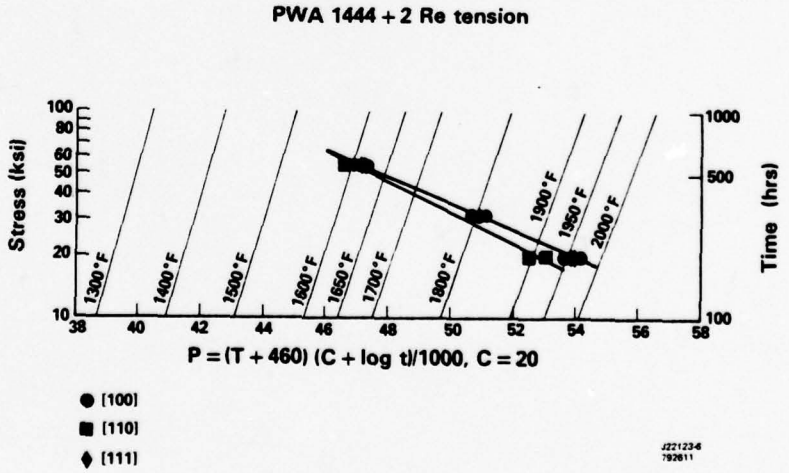

Figure 3-18 Larson-Miller Plots of High Symmetry Orientations of Alloy 1444 + 2 Re for Failure Condition.

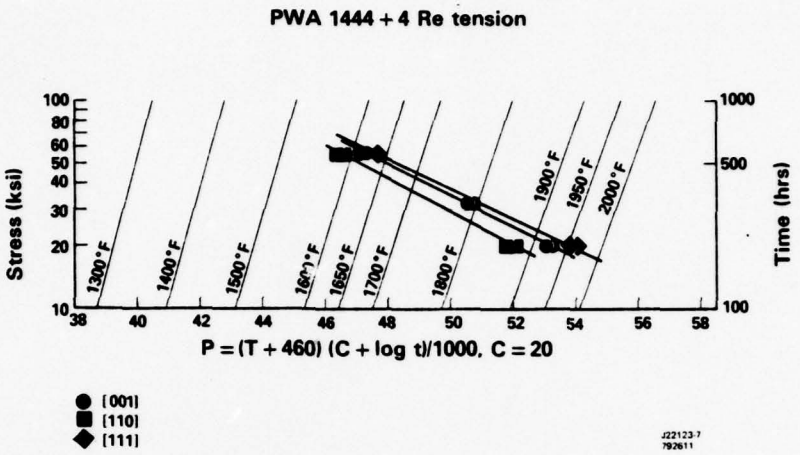

Figure 3-19 Larson-Miller Plots of High Symmetry Orientations of Alloy 1444 + 4 Re for Failure Condition.

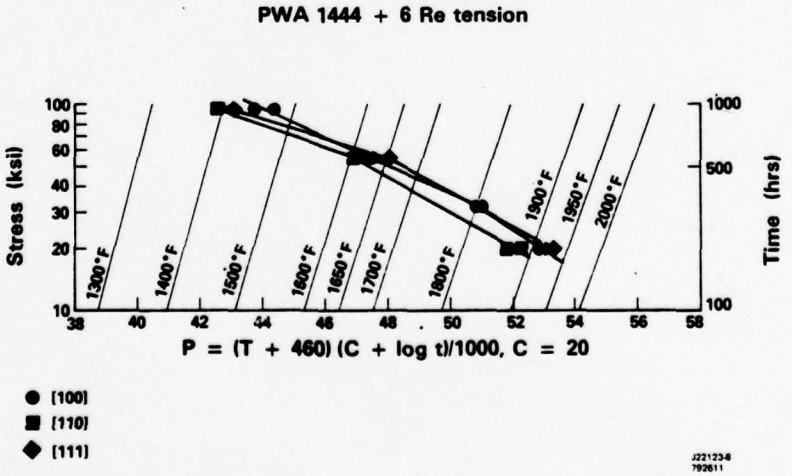

Figure 3-20 Larson-Miller Plots of High Symmetry Orientations of Alloy 1444 + 6 Re for Failure Condition.

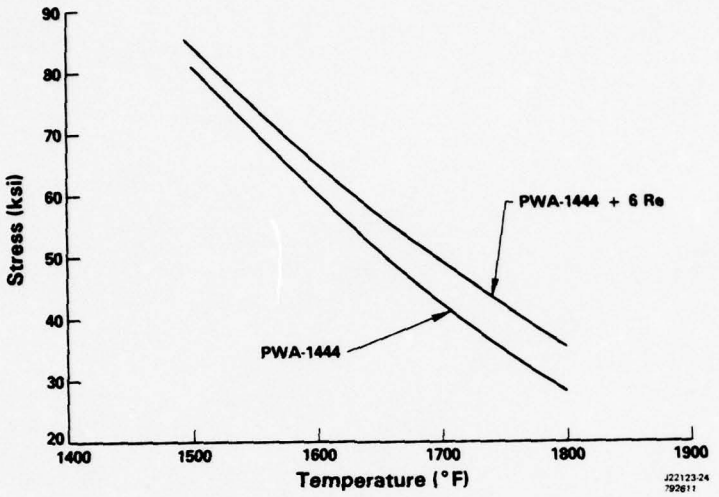

Figure 3-21 Stress for 1% Tensile Creep in 100 Hr. for < 001 > Alloy 1444 and 1444 + 6 Re.

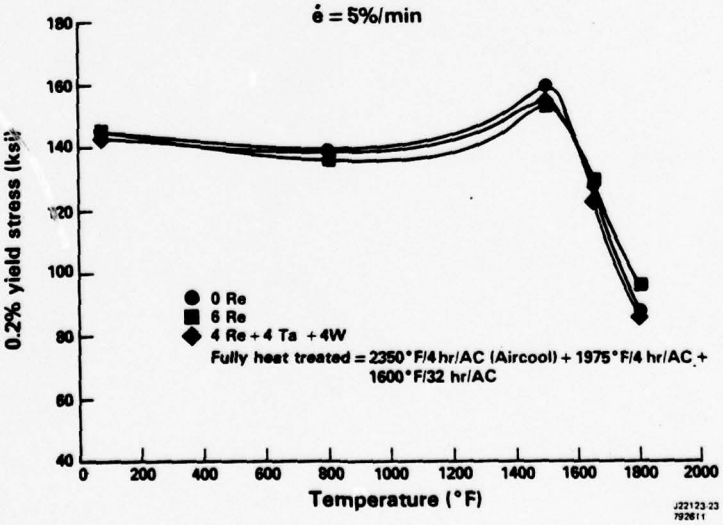

Figure 3-22 [001] Compressive Yield Strength Versus Temperature for Several Modifications to Alloy 1444.

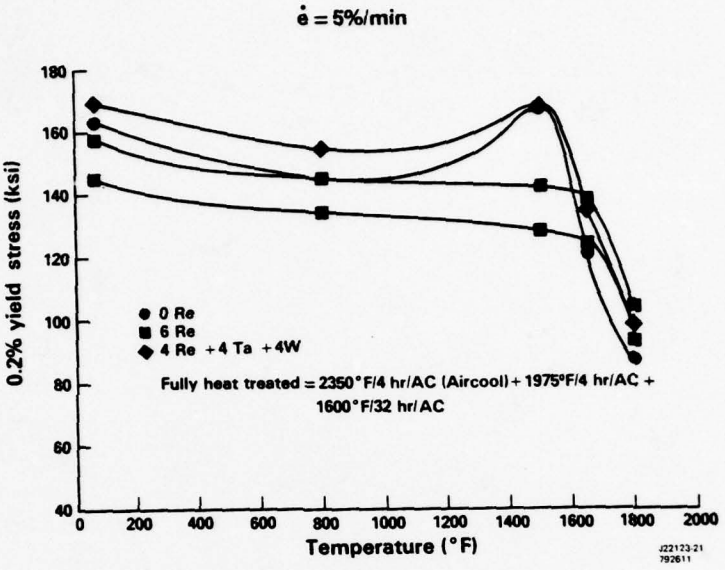

Figure 3-23 [110] Compressive Yield Strength Versus Temperature for Several Modifications to Alloy 1444.

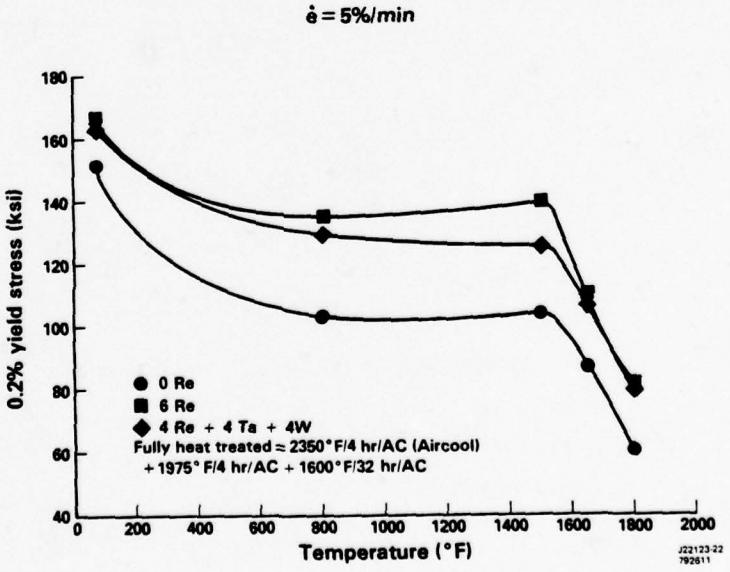

Figure 3-24 [111] Compressive Yield Strength Versus Temperature for Several Modifications to Alloy 1444. Note extreme weakness without Re Additions.

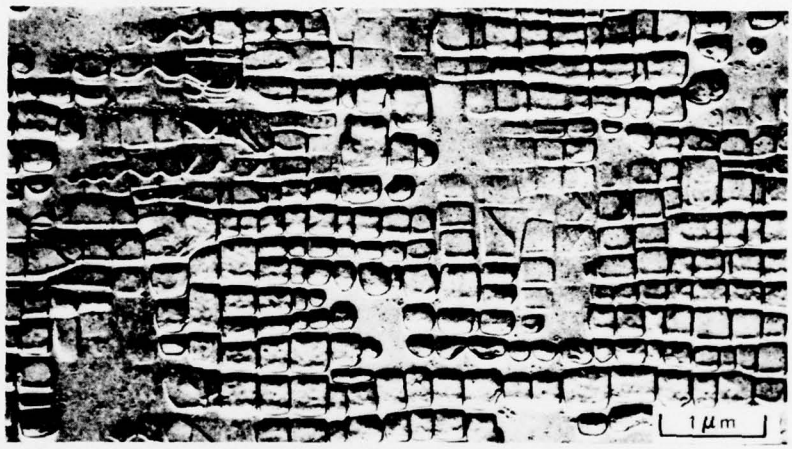

1444 +0 Re. Sol. HT +1950°F/2 hr

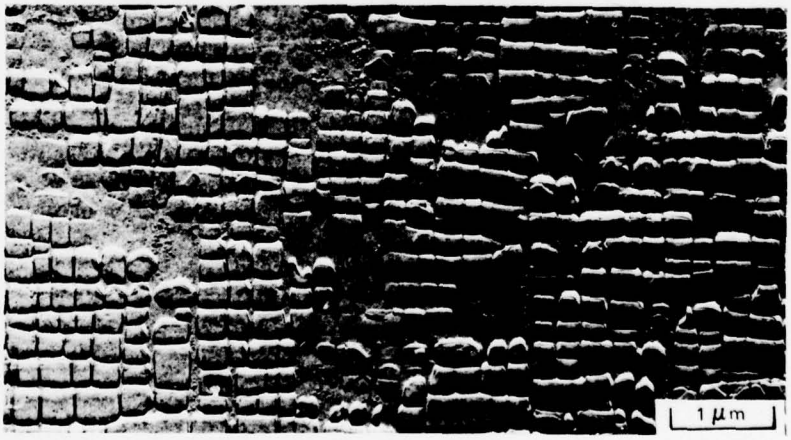

Figure 3-25 (001) Surface Replicas of 1444 and 1444 + Re Solution Heat Treated and Exposed to 1950°F/2 Hr.

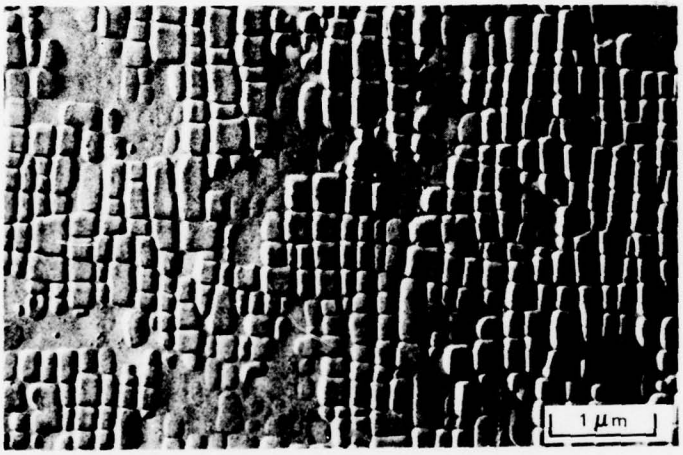

1444 + 4 Re. Sol HT + 1950°F/2 hr

1444 + 6 Re. Sol. HT + 1950°F/2 hr

Figure 3-26 (001) Surface Replicas of 1444 with 4 and 6 Re Solution Heat Treated and Exposed to 1950°F/2 Hr.

1444 + 0 Re. Sol. HT + 1500°F/296 hr

1444 + 2 Re. Sol. HT + 1500°F/296 hr

Figure 3-27 (001) Surface Replicas of 1444 and 1444 + 2 Re Solution Heat Treated and Exposed to 1500°F/296 Hr.

1444 + 4 Re. Sol. HT + 1500°F/296 hr

1444 + 6 Re. Sol. HT + 1500°F/296 hr

Figure 3-28 (001) Surface Replicas of 1444 with 4 and 6 Re Solution Heat Treated and Exposed to 1500°F/296 Hr.

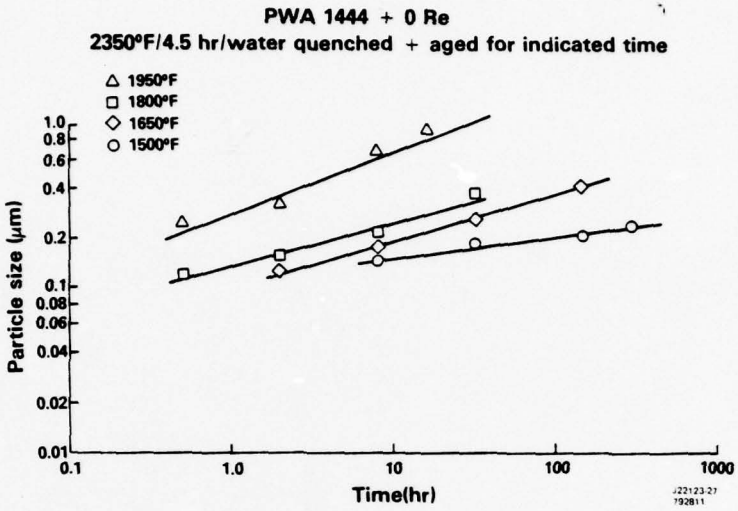

Figure 3-29 Isothermal Coarsening Kinetics for Alloy 1444 at Four Temperatures.

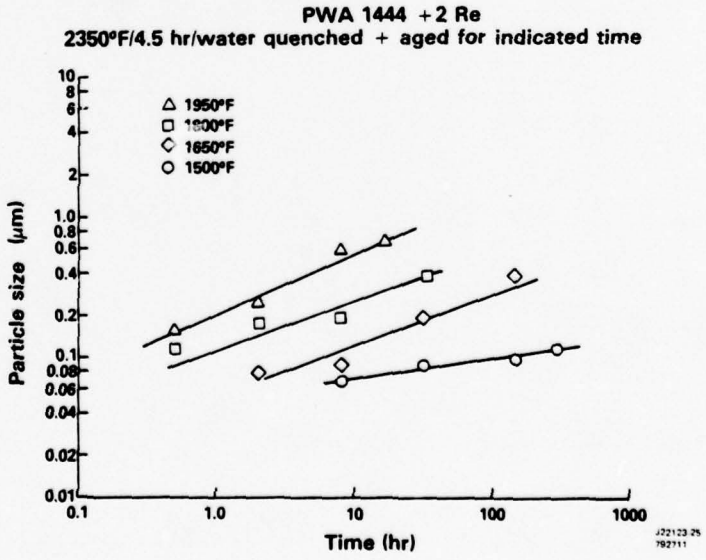

Figure 3-30 Isothermal Coarsening Kinetics for Alloy 1444 + 2 Re at Four Temperatures.

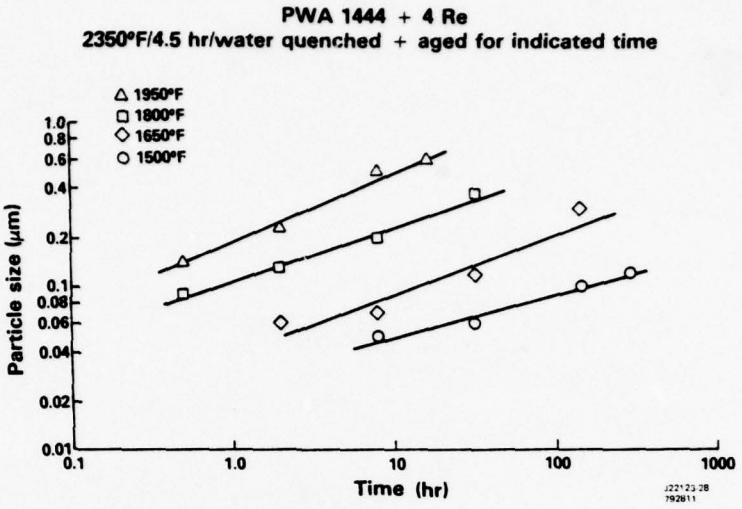

Figure 3-31 Isothermal Coarsening Kinetics for Alloy 1444 + 4 Re at Four Temperatures.

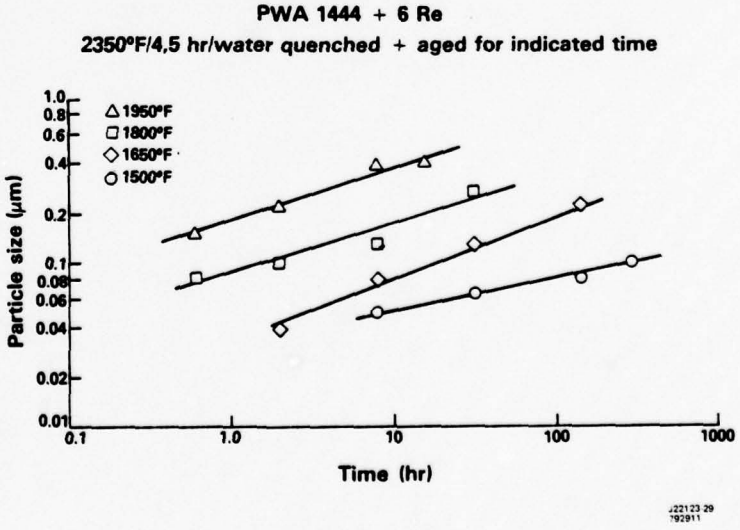

Figure 3-32 Isothermal Coarsening Kinetics for Alloy 1444 + 6 Re at Four Temperatures.

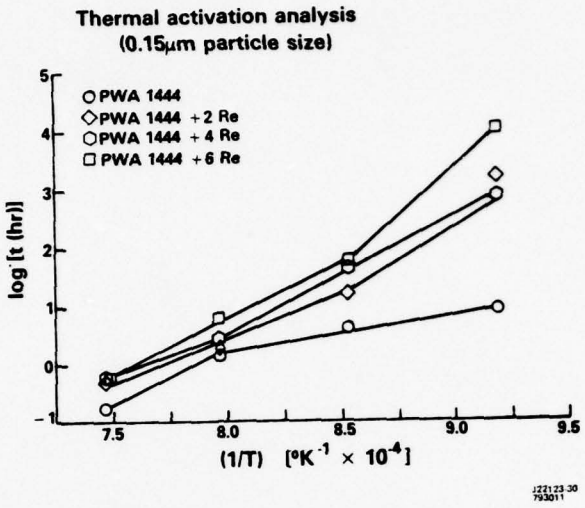

Figure 3-33 Thermal Activation Analysis of Time to Achieve a 0.15 μm γ' Particle Size for Four Re Levels in Alloy 1444.

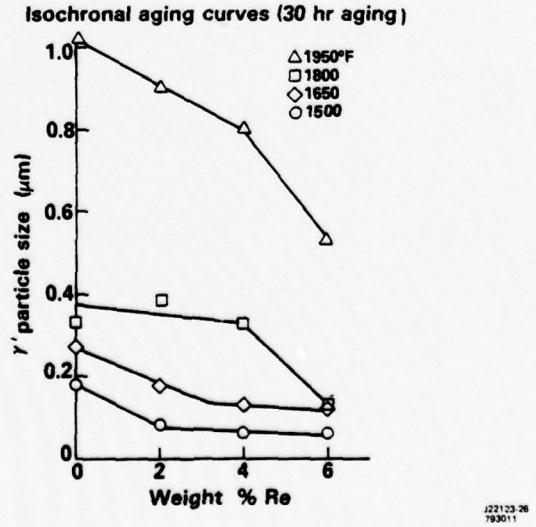

Figure 3-34 Isochronal Aging Plots for γ' Particle Size After 30 Hr. Aging Time Versus Re Level for Four Temperatures.

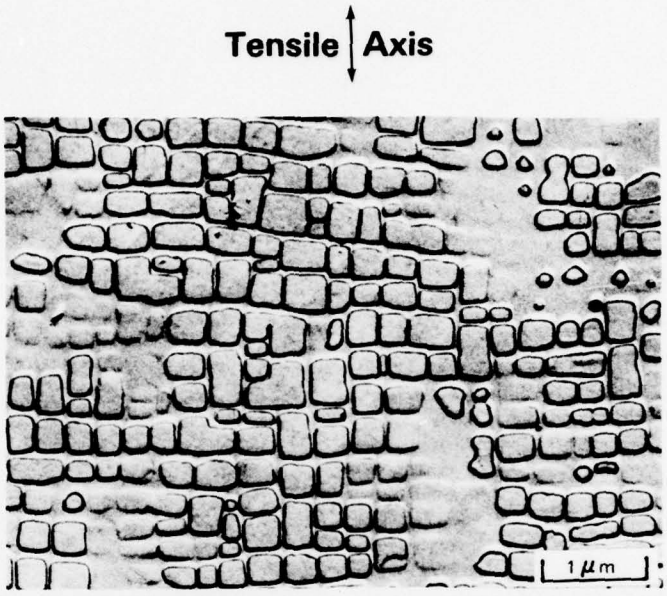

1650°F/55 ksi, 6 Re, [001]

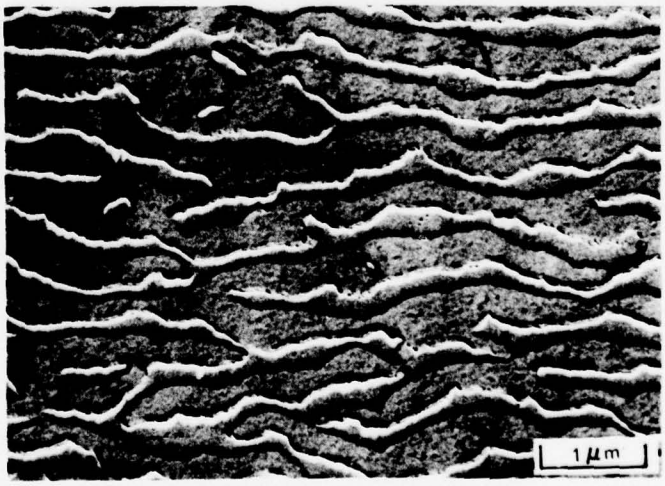

1800°F/32 ksi, 6 Re, [001]

Figure 3-35 Stress Coarsening Results at Two Temperatures/Stress Combinations for 6 Re.

Tensile ↕ Axis

1950°F/20 ksi, 6 Re, [001]

1950°F/20 ksi, 0 Re, [001]

Figure 3-36 Stress Coarsening Replicas Longitudinal to [001] at 1950°F/20 Ksi for 1444 and 1444 + 6 Re.

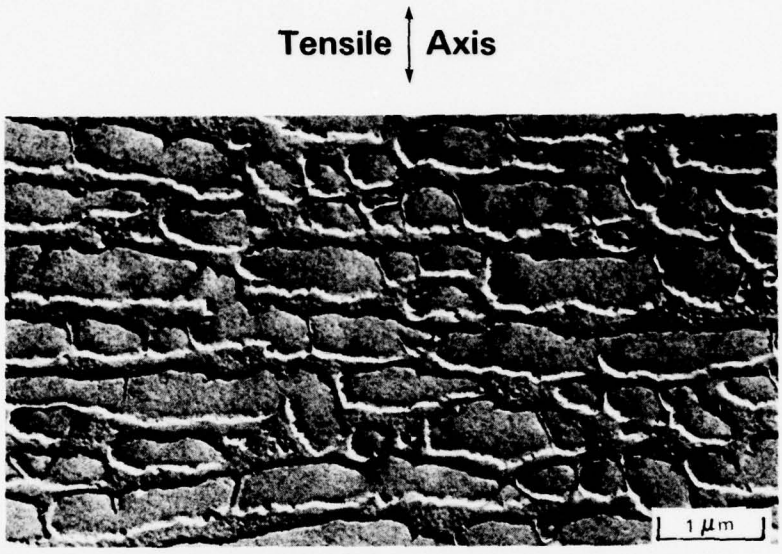

1950°F/20 ksi, 6 Re, [110]

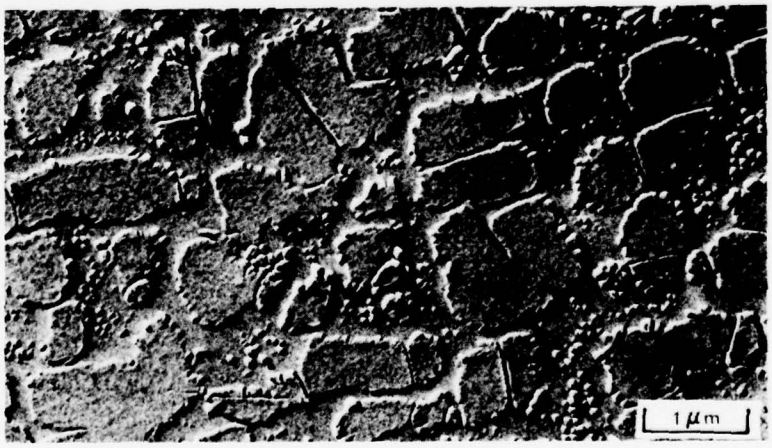

1950°F/20 ksi, 6 Re, [111]

Figure 3-37 Stress Coarsening Replicas Longitudinal to [110] and [111] Tensile Axes for 1444 + 6 Re Exposed to 1950°F/20 Ksi.

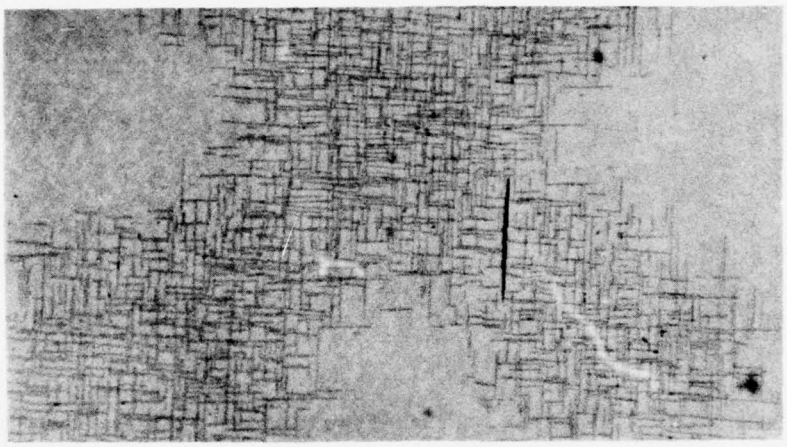

500X

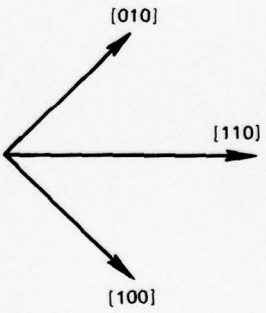

1000X

Figure 3-38 Transverse Micrographs From 1444 + 6 Re [001] Specimen Taken to Rupture at 1950°F/20 Ksi.

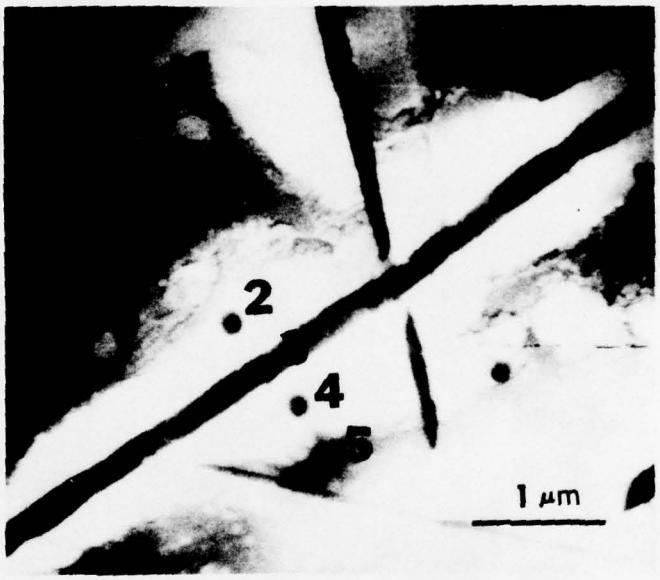

Contamination spots where specimen was analyzed

Spot no. 3 in sigma phase

Figure 3-39 STEM Analysis from Thin Foil Taken Transverse to < 111 > 1950/20 Ksi Creep Rupture Specimens from 1444 + 4 Re.

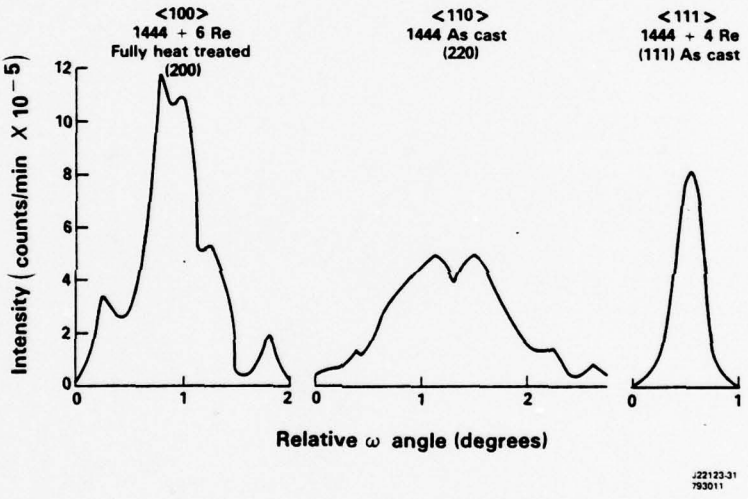

Figure 3-40 Omega Scans for Transverse Crystals Cut From Three Bars with Various Growth Axes

Figure 3-41 Backscattered and Secondary Electron Images (BEI and SEI) from (001) Transverse Cut of < 001 > PWA 1444 Bar. Two electron channeling photos are shown with 200 μm translation and a noticable orientation difference. SEI contrast outlines substructure as related to dendrite groupings.

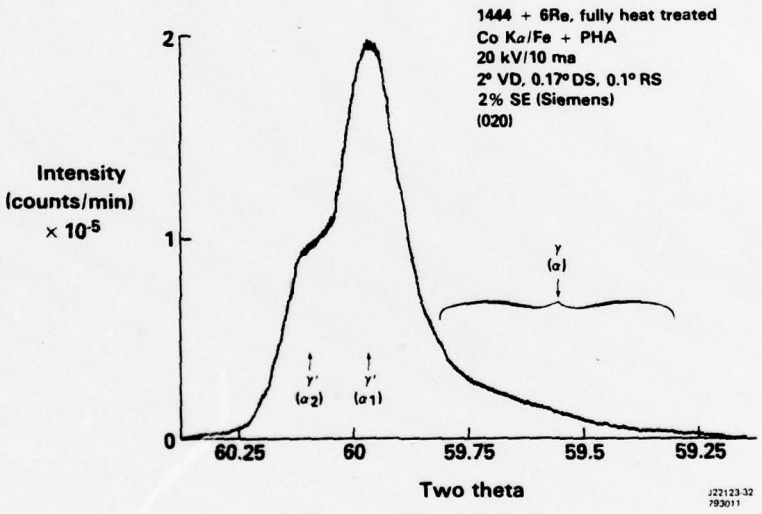

Figure 3-42 $\theta/2\theta$ Trace from Vertical Section of <001> Single Crystal Bar of 1444 + 6 Re

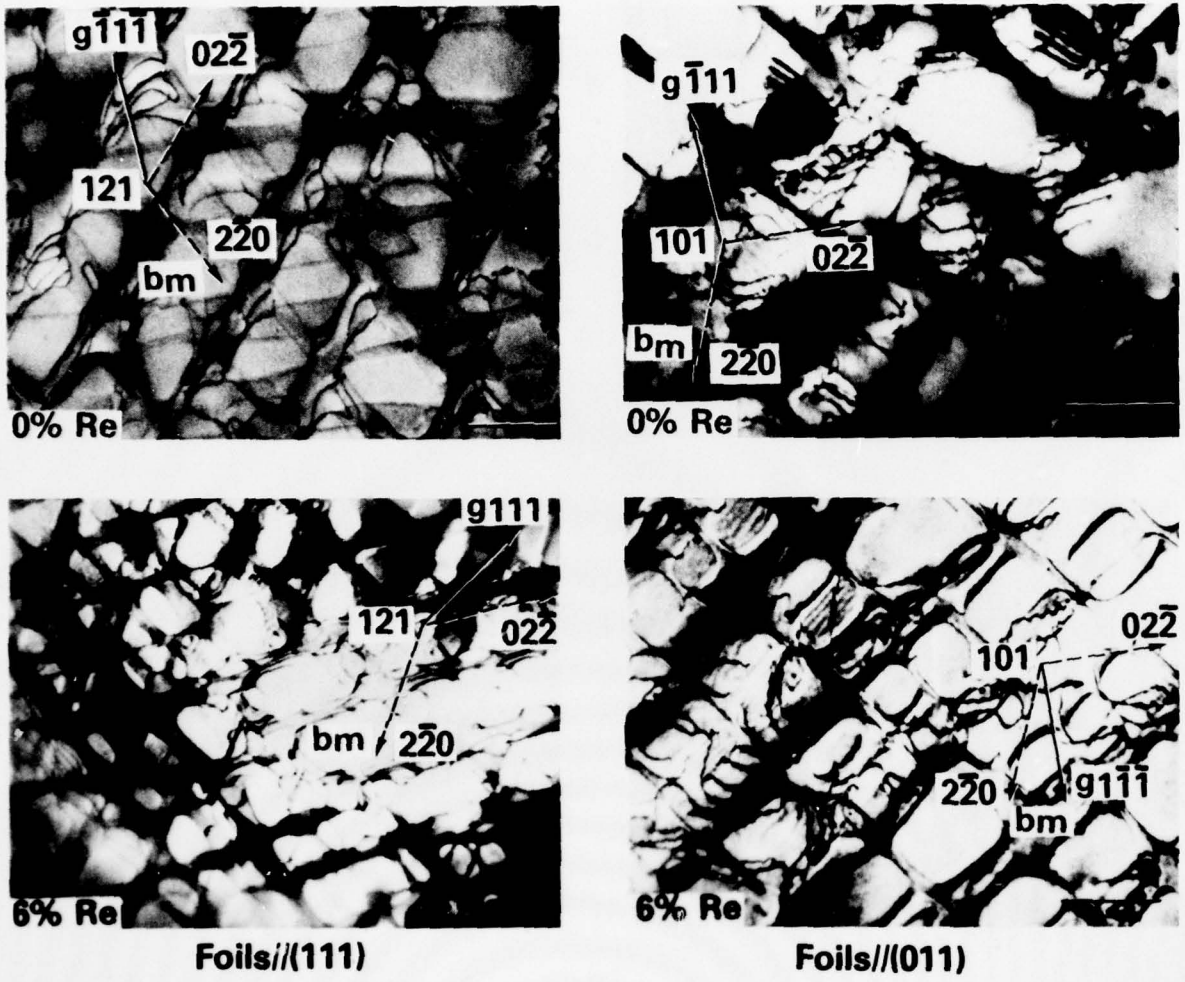

Figure 3-43 Thin Foils and Slip Vector Analyses for [011] Tensile Creep at 1650°F/55 Ksi for Alloy Base 1444, with Various Re Additions.

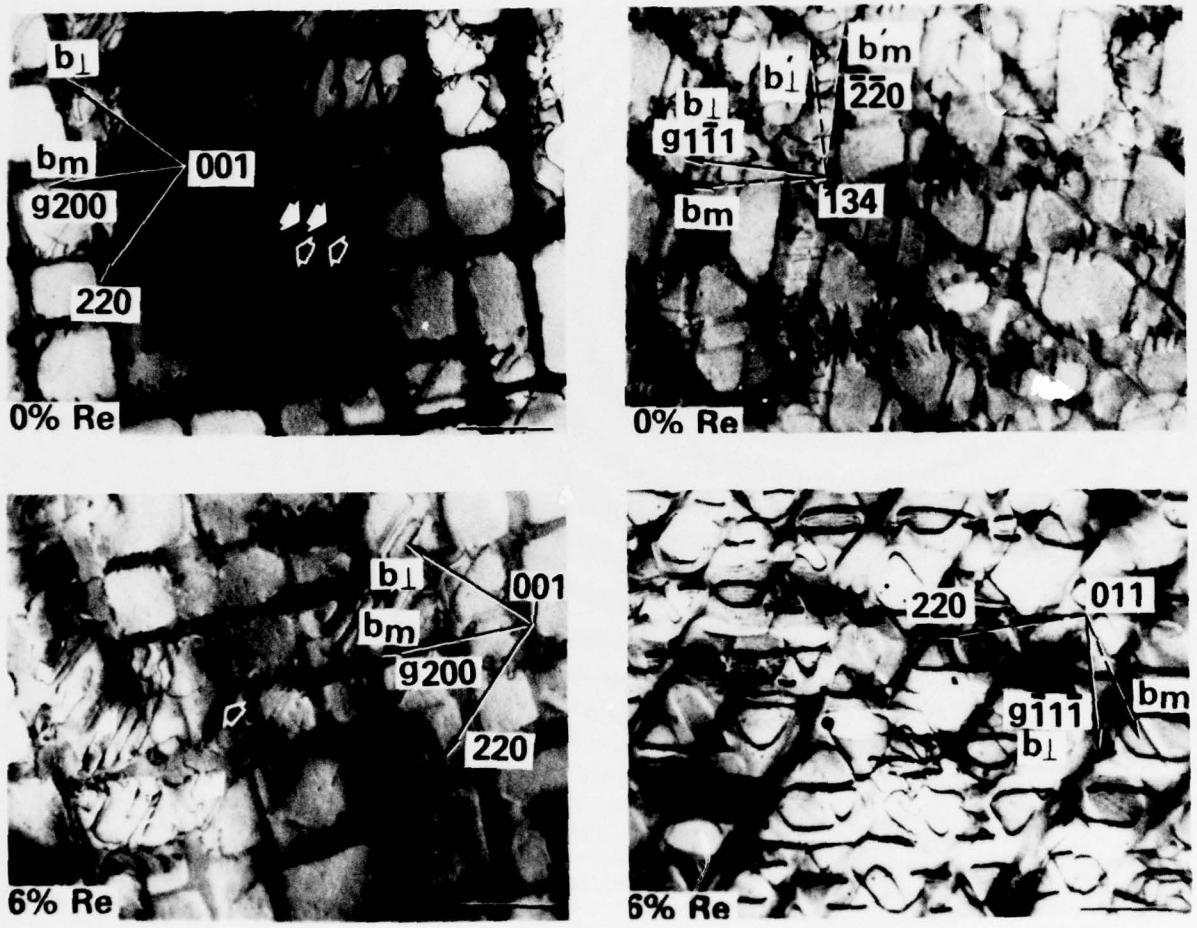

Figure 3-44 Thin Foils and Slip Vector Analyses for [111] Tensile Creep at 1650°F/55 Ksi for 1444 with Various Re Additions.

Figure 3-45 Thin Foils from Compressive Creep for Various Orientations and Re levels at 1650°F/55 Ksi

4.0 Discussion

The creep data at four temperatures, five compositions, three orientations and two stress senses were generally well behaved. The only exceptions were <110> tension at 1500°F and all orientations at 1950°F for 4 and 6 wt% Re. Since the compressive data were systematic (and the primary creep strains were in the reasonable range of 0.3 to 2.0%), it can be concluded that <110> in tension at 1500°F/94 ksi represents an overstressed condition, and the specimens undergo runaway creep on a single glide system. In a compression test, with end constraints, or in a multi-axial "real world" application, such behavior may never occur, but is of some concern nonetheless.

This same orientation shows good compressive creep resistance and a high yield strength (in compression) at 1500°F, which is consistent with the anticipated width of a γ' complex fault for <110> according to recent work(10). This may also explain the excellent <110> compressive creep resistance, see Figure 3-17.

The aforementioned anomalous behavior at 1950°F can be explained in terms of the σ phase instability. This phase may not form at 2% Re, or may only form in residual pockets of microsegregation, or may form on such a fine scale that it provides strength rather than weakness. Beyond 2% Re, however, the higher the Re, the greater the amount and length of platelets and the shorter the life. The degredation of creep properties can be directly associated with a substantial depletion of the Re level in the γ phase as σ is formed.

It may be worthwhile to point out that the σ forms despite the fact that the alloys are of proper chemistry and that all creep specimens were fully heat treated. The σ phase always formed in dendrite cores, however, and this is consistent with the chemistry which was determined and the fact that the liquid/solid distribution coefficient for Re is much greater than unity (as is the case for W). This combined with the large atom size for Re and the low diffusivity, leads to residual microsegregation even after solution heat treatment. It is important to point out that the inherent 1950°F alloy instability may lead to hyperfine precipitates or atmospheres around dislocations at the lower temperatures, and this is a possible contribution to the Re strengthening effect which cannot be ruled out. However, the anisotropy of the effect would suggest other factors are more important.

A few comments are also in order regarding compressive creep as an experimental tool. If the length to width ratio is 3:1 to 4:1, we have found the data to be well behaved, systematic and reproducible, but generally with 2X to 5X lower creep rates than tension. One reason for this difference may be the influence of tiny solidification micropores on tensile creep due to vacancy generation. The compressive creep data may represent the ultimate performance potential of a virtually perfect material. As a research tool, this may be particularly significant. The trouble with defects such as pores (or inclusions) is that they cannot be reproduced from sample to sample. This concept is entirely consistent with the very low scatter in compressive MCR vs. tensile for this work, or for single crystals in general. It should also be pointed out that the compressive data were gathered in a hydraulic

closed loop system and a furnace with excellent temperature control. The Lucalox loading buttons and alumina rams can be considered non-deformable at the temperature/stress combinations employed. The compressive strain measurements were made dynamically using the Lucalox buttons as reference via clamped differential extension rods and an LVDT set-up for continuous analog output. It is possible that this type of testing is inherently more accurate than a leveraged creep frame with significant vibration and friction, deformable grips, temperature oscillation (and drift due to the use of chromel/alumel rather than the Pt/Rh used in the compression rig).

The Re effect on isothermal coarsening without stress has been fully documented and is particularly significant when viewed as the time to reach a given particle size at a given temperature. In terms of the Re strengthening effect, this delays overaging and independent slip in γ and γ' and forces the two phases to slip in a mutually compatible manner. This is the condition for optimum strength since cutting of the γ' is required. Another effect of the Re in preventing obstacle avoidance is the generation of a finer stress coarsened γ' lamellar structure at 1800 and 1950°F. Such rafts are common at high temperature on a coarse scale, but the Re keeps the inter-lamellar spacing fine, which again forces the dislocations to cut through both phases and independent slip, bowing between, and climbing around γ' are circumvented.

The <111> effects are the most dramatic and certainly the key to the Re effect. We know that Re partitions to the matrix as the γ' grows. We have seen mechanical and microstructural evidence for cube slip, {001} <110>, in the <111> 0 Re tensile creep specimens. The addition of Re must force the <110> shear to stay on octahedral planes. This effect is not in the γ', since there is scarcely any Re in that phase. There is still a question of whether the slip initiates in the matrix on {001} or {111}. Cube slip is very common in γ', but only rarely seen in the γ matrix. The 1444 matrix composition may just be susceptible to cube slip, and the Re may counteract this weakness by lowering the stacking fault energy (similar to chromium). 1444 without Re shows <111> weakness at intermediate temperature. The γ' is always susceptible to cube slip (due to low anti-phase boundary energy), so it must be the γ without Re which is so weak. The γ may even still initiate slip on {111}, but quickly cross-slip to {001}, since the <001>tensile and compressive creep data are so well behaved.

The measured misfit may play a small role in the general creep improvement as Re is added. It must be admitted that the room temperature measurement may not be identical to the high temperature misfit, but is worthy of note because of the unusually large magnitude and reverse sense to normal behavior which should be preserved at elevated temperature. The negative misfit is presumably due to the substantial accumulation of Re in γ'. At 60 vol % γ', 6% Re in the alloy becomes approximately 15% in the γ phase with no γ' solubility for Re. This substantial amount could lead the large negative misfit (as well as big effects on stacking fault energy and solid solution strengthening). One interesting fact concerning the thermal and constitutional dependence of the in-situ misfit is the observation that the γ' particles are more regular and cuboidal at high Re and/or high temperature. This

does not indicate the sign of the misfit, but it does show that the misfit does not disappear. γ' being relatively free of Re has reasonably well known thermal expansion, but the effect of Re on the thermal expansion characteristics is unknown. Ni-Re may be anomalous in a fashion similar to Ni-Cr alloys. We can conclude that the misfit is probably still negative, but moderate in magnitude at high Re in the intermediate temperature range since the γ' particles are regular and do not show rapid coarsening which would be associated with high energy interfaces.

The 4Re/4Ta/4W alloy was included primarily because Re and W have distribution coefficients greater than unity, but that for Ta is less than unity. The Ta presumably strengthens the γ' while the Re strengthens the γ. This alloy was not unusually strong, indicating segregation is not playing a key role. The crystal perfection was not significantly different from the other four alloys studied. The only dramatic change in crystal quality was the high degree of perfection in <111> . This is due to the fact that there is relative motion within the dendrite field on cube planes (as indicated by visual observation, ω-χ maps and electron channeling studies. In <001> or <110> there are vertical cube planes which tend to propagate the imperfections, but in <111>, the inclination of the cube planes tends to make any defects associated with primary dendrite shifts to quickly grow out without perpetuation or accumulation. The high resultant crystal quality may actually favor slip on only one system. This was often observed in <111> (as well as substantial sensitivity to inclusions). <001> always showed multiple systems, mixed character dislocations and intersecting slip with excellent ductility.

It seems appropriate to summarize the key findings of this investigation of single crystal anisotropy as follows:

(1) At 1800°F/32 ksi the orientation dependence of creep properties was not significant near <001> with a slight improvement in creep resistance with misorientation up to 20°.

(2) The <110> and <111> high modulus orientations of alloy 1444 (5Al, 2Ti, 1Cb, 9Cr, 12W by wt. in Ni) were grown as seeded single crystals and tested in tensile creep as well as compressive yield strength.

3) Various Re additions were made for W, and Re was found to systematically strengthen the 1444 base, especially for the <111> orientation. Testing was carried out in three orientations, five compositions, two stress senses and four combinations of temperature and stress. Compressive yield strength was also measured as a function of composition, orientation and temperature.

4) Isothermal γ' coarsening rates were documented and stress coarsening was observed. The Re additions led to significantly finer γ' structures.

5) Thin foil analysis indicated predominantly {111} <110> slip with <112> occurring only rarely and {100} <110> taking place with a <111> tensile axis.

6) Compressive single crystal superalloy creep was highly developed as a laboratory tool to study the influence of chemistry on creep rates with an excellent degree of reproducibility. The tensile creep rate also showed little scatter for single crystals as compared to typical multi-grained alloys.

7) The powerful Re strengthening effect can be attributed to the following list of documented changes in microstructure or chemistry (listed in their probable order of importance):

   a) suppression of tendency for cube slip

   b) refinement of microstructure

   c) γ phase solid solution strengthening

   d) γ' large negative misfit and tetragonal distortion

   e) pre-precipitation "atmospheres"

4.1 Acknowledgement

This multi-year effort involved several closely related topics investigated by G. R. Leverant, M. Gell, D. N. Duhl and the current author. These individuals are cited here for their contribution to an improved understanding of mechanical property alloy anisotropy in advanced high temperature alloy systems. In the last two years of work, R. E. Doiron and J. Lin contributed substantially to the smooth flow of mechanical testing and microstructural analysis.

5.0 REFERENCES

1. G.R. Leverant and B.H. Kear, Met. Trans., Vol. 1 (1970), p. 491.

2. G.R. Leverant, B.H. Kear and J.M. Oblak, Met. Trans., Vol. 4 (1973), p. 355.

3. G.R. Leverant, B.H. Kear and J.M. Oblak, Met. Trans., Vol. 2 (1971), p. 2305.

4. G. Dieter, "Mechanical Metallurgy", McGraw-Hill (1961).

5. A.F. Giamei and J.S. Erickson, Proceedings Third International Symposium on Superalloys, Seven Springs, Pa., Claitor's Publ. Div., Baton Rouge, LA., September 1976, p. 405.

6. H.D. Brody and A.F. Giamei, AFML Contract F33615-75-C-5204, June 1975-June 1977.

7. D.J. Chellman and A.J. Ardell, Acta Met., Vol. 22 (1974), p. 577.

8. V. Murjal and A.J. Ardell, Acta Met., Vol. 23 (1975), p. 513.

9. L.M. Brown and R.K. Ham, "Strengthening Methods in Crystals", ed. by A. Kelly and R.B. Nicholson, Elsevier Publ. Co., Amsterdam, 1971, p. 9.

10. C. Lall, S. Chin and D. Pope, Met. Trans. A (1979), p. 1323.

11. P.R. Strutt, M. Khobaib, R.S. Polvani and B.H. Kear, Proc. Fourth International Conference on Strength of Metals and Alloys, Nancy France, September 1976, p. 314.

12. B.H. Kear, A.F. Giamei, J.M. Silcock and R.K. Ham, Scripta Met., Vol. 2, No. 5 (1968), p. 287.

13. B.H. Kear, A.F. Giamei and J.M. Oblak, Scripta Met., Vol. 2, No. 11 (1968), p. 597.

14. B.H. Kear, A.F. Giamei, G.R. Leverant and J.M. Oblak, Scripta Met., Vol. 3, No. 2 (1969), p. 123.

15. B.H. Kear, A.F. Giamei, G.R. Leverant and J.M. Oblak, Scripta Met., Vol. 3 (1969), p. 455.

16. B.H. Kear, A.F. Giamei and J.M. Oblak, Scripta Met., Vol. 4, No. 8 (1970), p. 567.

17. B.H. Kear, J.M. Oblak and A.F. Giamei, Proceedings, Second International Conference on Strength of Metals and Alloys, ASM, Cleveland, Ohio (1970), p. 1155.

REFERENCES (Cont'd)

18. A.F. Giamei, J.M. Oblak, B.H. Kear and W.H. Rand, Proceedings 29th Annual EMSA Meeting, Claitor's Publ. Div., Baton Rouge, LA., (1971) p. 112.

19. J.E. Doherty, A.F. Giamei and B.H. Kear, Met. Trans. A (1975), p. 2195.

20. C.C. Law and A.F. Giamei Met. Trans. A. (1976), p. 5.

21. A.E. Staton-Beran and R.D. Rawlings, Phys. Stat. Sol. (a), Vol. 29 (1975), p. 613.

22. L. Woodyatt, C. Sims and H. Beattie, Jr., Trans. TMS-AIME (1966), P. 519.

6.0 PUBLICATIONS AND PRESENTATIONS FROM AFOSR SPONSORED WORK

- A presentation of progress to date was made to I. Machlin's joint DOD/NASA committee on D.S. Eutectics at NAV AIR in Washington, D.C. on March 4, 1976.

- A paper entitled "The Anisotropy of Deformation and Fracture in a Directionally-Solidified Ni/Ni_3Cb Lamellar Eutectic Alloy" was published in Metallurgical Transactions, Vol. 8A, Jan., pp. 83-89.

- A presentation entitled "The Anisotropy of Deformation and Fracture in the Directionally Solidified Ni/Ni_3Al-Ni_3Cb Eutectic Alloy" was made at the Fall Meeting of TMS-AIME, Niagara Falls, N.Y. in September.

- A presentation on the orientation dependence of creep rates was made in the Fall Meeting of TMS-AIME, Milwaukee, Wis. in October 1979.

- A presentation of the effects of Re on superalloy deformation was made at the Fall Meeting of TMS-AIME in Milwaukee, Wis., October, 1979.

7.0 TECHNICAL PERSONNEL

The proposed effort will be conducted by Dr. Anthony F. Giamei of MERL. His biographical sketch and List of Publications are given in sections 7.1 and 7.2.

7.1 BIOGRAPHICAL SKETCH

ANTHONY F. GIAMEI

Pratt & Whitney Aircraft Group - Commercial Products Division

Position: Senior Staff Scientist and Head of the Casting Technology Research and Development Group of the Materials and Process Development and Research Section of the Materials Engineering and Research Laboratory.

Area of Responsobility: Dr. Giamei is responsible for conducting research in the areas of strengthening, working and solidification of Ni-base superalloys, and determining the implications of such fundamental studies on high temperature alloys and processing techniques.

Direct Program Related Experience: Thirteen years of professional experience in the areas of research and development of advanced high temperature alloys and directional solidification processing. Special interests have included monocrystal growth and characterization of commercial and advanced superalloys and eutectics. Recent work has emphasized heat transfer, thermal analysis, segregation and high thermal gradient or high solidification rate crystal growth. Additional activities include electron beam melting, computerized analysis and process control, seeded crystal growth and high temperature alloy strength studies.

Management/Technical Experience:

1977 - Supervisor of the Casting Technology Research and Development Section

1974 to 1977 - Supervisor of the Solidification Research Group in the Casting Development Section of the Materials Engineering and Research Laboratory.

1973 - Supervisor of the Turbine Materials Synthesis Group in the Compressor and Turbine Materials Section of the Materials Engineering and Research Laboratory.

1966 to 1973 - Research Associate and Senior Research Associate in the Alloy Studies Group of the Alloy and Materials Development Section of the Advanced Materials Research and Development Laboratory, Pratt & Whitney Aircraft, as noted above.

Education:

1966 - Northwestern University, Doctor of Philosophy degree in Materials Science. Dr. Giamei was awarded a Walter P. Murphy Fellowship for one year, a National Science Foundation Fellowship for two years, and a Cabell Memorial Fellowship for one year.

1962 - Yale University, Engineering School, Bachelor of Engineering degree. Dr. Giamei was awarded his degree with highest honors, and received the Calhoun Fellows Cup for academic distinction and the Prize for Excellence in Metallurgy.

Additional Information: Dr. Giamei is a Fellow of the American Society for Metals and past Chairman of the New Haven Chapter of the American Society for Metals, a member of the Advisory Technical Awarness Council of the American Society for Metals, past Chairman of the Solidification Committee and member of the High Temperature Alloys Committee of the American Institute of Mining, Metallurgical and Petroleum Engineers, a membe of Tau Beta Pi and Sigma Xi. He holds 15 U.S. Patents in the area of directional solidification, and is author or co-author of the following publications:

7.2 Publications

1. "Optimization of X-ray Diffraction Quantitative Analysis" (with E. J. Freise), Trans. TMS AIME 239, pp. 1676-1684, November 1967.

2. "The Role of the Allotropic Transformation in Cobalt-Base Alloys I" (with J. Burma and E. J. Freise), Cobalt No. 39, pp. 88-96, June 1968.

3. "The Role of the Allotropic Transformation in Cobalt-Base Alloys II" (with J. Burma, S. Rabin, M. Cheng and E. J. Freise), Cobalt No. 40, pp. 140-155, September 1968.

4. "Slip and Climb Processes in Precipitation Hardened Nickel-Base Alloys" (with B. H. Kear, J. M. Silcock and R. K. Ham), Scripta Met. 2, No. 5, pp. 287-294, May 1968.

5. "On the Nature of Intersection Jogs in the $L1_2$ Structure" (with B. H. Kear and J. M. Oblak), Scripta Met. 2, No. 11, pp. 597-604, November 1968.

6. "On Intrinsic/Extrinsic Stacking Fault Pairs in the $L1_2$ Lattice" (with B. H. Kear, G. R. Leverant and J. M. Oblak), Scripta Met 3, No. 2, pp. 123-130, February 1969.

7. "Viscous Slip in the $L1_2$ Lattice" (with B. H. Kear, G. R. Leverant and J. M. Oblak), Scripta Met. 3, 455-460 (1969).

8. "On the Nature of Freckles in Nickel-Base Superalloys" (with B. H. Kear), Met. Trans. 1, No. 8, pp. 2185-2192, August 1970.

9. "On the Origin of Freckles in Unidirectionally Solidified Castings" (with S. M. Copley, S. M. Johnson and M. F. Hornbecker), Met. Trans. 1, No. 8, pp. 2193-2204, August 1970.

10. "On the Origin of Stacking Faults in Plastically Deformed Ni_3Al (Phase)" (with B. H. Kear and J. M. Oblak), Scripta Met. 4, No. 8, pp. 567-574, August 1970.

11. "Stacking Faults in Gamma Prime $Ni_3(Al,Ti)$ Precipitation Hardened Nickel-Base Alloys" (with B. H. Kear and J. M. Oblak), Met. Trans. 1, No. 9, pp. 2477-2486, September 1970. Note: Received the New England Regional Conference of AIME Award for the outstanding technical paper of 1970 submitted from New England.

12. "Slip Viscous Slip and Climb Processes in Precipitation Hardened Nickel-Base Alloys" (with B. H. Kear and J. M. Oblak), Proceedings of the Second International Conference on the strength of Metals and Alloys, Vol. III, pp. 1155-1159, ASM, Cleveland, Ohio (1970).

13. "The Formation of Crystallographically-Aligned a/3 112 Dislocations in Ni_3Al" (with J. M. Oblak, B. H. Kear and W. H. Rand), Proceedings of the 29th Annual Meeting, EMSA, pp. 112-113, Claitor's Publ. Div., Baton Rouge, La. (1971).

14. "On the Origin of Ductility Enhancement in Hf-Doped Mar-M200" (with J. E. Doherty and B. H. Kear), J. Met. 23, pp. 59-62, November 1971.

15. "Morphology of Precipitates in Ni-Rich -Ni_3 (Al, Ta)" (with B. H. Kear, J. E. Doherty and L. P. Lemaire), Proceedings of the 30th Annual Meeting, EMSA, pp. 588-589, Claitor's Publ. Div., Baton Rouge, La. (1972).

16. "Dependence of Intergranular Fracture on Boundary Topography and Cohesion" (with J. E. Doherty, B. H. Kear and C. W. Steinke), Proceedings of the 31st Annual Meeting, EMSA, pp. 150-151, Claitor's Publ. Div., Baton Rouge, La. (1973).

17. "Transverse Grain Boundary Strengthening in a Directionally Solidified Nickel-Base Alloy" (with B. H. Kear and J. E. Doherty), Proceedings of the Third International Conference on the Strength of Metals and Alloys", Vol. I, pp. 134-138, Institute of Metals and the Iron and Steel Institute, Cambridge, England (1973).

18. "Precipitation of in the of Nickel-Base Superalloys" (with J. M. Oblak, J. E. Doherty and B. H. Kear), Met. Trans. 5, pp. 1252-1255, May 1974.

19. "Confirmation of Sulfur Embrittlement in Nickel Alloys" (with W. C. Johnson, J. E. Doherty and B. H. Kear), Scripta Met. 8, pp. 971-974 (1974).

20. "Control of Grain Boundaries for Structural Applications" (with F. L. VerSnyder), Proceedings of the 4th Bolton Landing Conference, pp. 3-26, Claitor's Publ. Div., Baton Rouge, La. (1974).

21. "The Importance of Grain Boundary Morphology and Cohesion on Intergranular Strength" (with J. E. Doherty and B. H. Kear), Can. Met. Quarterly, 13, pp. 229-236, March 1974.

22. "The Art and Science of Unidirectional Solidification" (with E. H. Kraft and F. D. Lemkey), in New Trends in Materials Processing, pp. 48-97, Amer. Soc. for Metals 1976.

23. "The Effect of Surface Chemistry in Grain Boundary Strength" (with J. E. Doherty, B. H. Kear and C. W. Steinke), Proceedings of the 4th Bolton Landing Conference, pp. 619-628, Claitor's Publ. Div., Baton Rouge, La. (1974).

24. "Directional Solidification of Superalloys" (with C. P. Sullivan and F. L. VerSnyder), Proceedings of the 5th International Symposium on Electroslag and other Special Melting Technologies-Part III, edited by G. K. Bhat and A. Simkovich, pp. 525-594, Carnegie-Mellon Institute of Research, Pittsburgh, Pa. (1975).

25. "Influence of Differential Dislocation Mobility on the Fatigue Behavior of Alloyed " (with J. E. Doherty and B. H. Kear), Metallurgical Transactions A, pp. 2195-2199, December 1975.

26. "Plastic Anisotropy of Directionally Solidified Nickel-Base Superalloys with Columnar-Grained and Monocrystal Structures in Conventional and Plane-Strain Compression" (with C. C. Law), Metallurgical Transactions A, pp. 5-16, January 1976.

27. "An Investigation of Directional Solidification of Ni_3Cb Reinforced Eutectics in Complex Shapes" (with P. M. Curran, L. F. Schulmeiser and J. S. Erickson), Conference on In-Situ Composites II, Bolton Landing, September 1975.

28. "Liquid Metal Cooling: A New Solidification Technique" (with J. G. Tschinkel), Metallurgical Transactions A, September 1976.

29. "Computer Applications in Directional Solidification Processing" (with J. S. Erickson), Third Int'l. Symp. on Superalloys, Seven Springs, PA, pp. 405-424, September 1976.

30. "Alloy Design and Processing of Advanced Directionally Solidified Eutectics" (with F. D. Lemkey), Japan-U.S. Joint Seminar on Solidification of Metals and Alloys, Tokyo, Japan, pp. 240-255, January 1977.

31. "Inhomogeneous Deformation of Nickel-Base Superalloy 111 Monocrystals under Compression" (with C. Law and A. V. Karg), J. Mat. Sci. and Eng'g., 29, No. 1, pp. 29-35, July 1977.

32. "Microsegregation and Homogenization of Ni-7.5 wt % Al-2.0 wt% Ta Dendritic Monocrystals", (with G. D. Merz and T. Z. Kattamis), J. Mat. Sci., 14, pp. 663-670, 1979.